

Description of the
Fourth Concept Detector ("4th") for the
International Linear Collider

Emanuela Cavallo, Vito Di Benedetto, Corrado Gatto, Franco Grancagnolo,
Anna Mazzacane, Roberto Perrino
INFN and Dipartimento di Fisica, Universita' degli Studi di Lecce
via Lecce-Arnesano, 73100, Lecce, Italy

Aldo Penzo
INFN, Trieste
Padriciano 99; I-34012 Padriciano, Trieste, Italy

Giovanni Pauletta¹
University di Udine
33100 Udine, UD, Udine, Italy

Sunghwan Ahn, Tae Jeong Kim, Kyong Sei Lee, Sung Keun Park
Department of Physics, Korea University
Seoul 136-701, Korea

Sorina Popescu², Laura Radulescu
IFIN-HH
Bucharest, Romania

Sezen Sekmen, Efe Yazgan¹, Mehmet Zeyrek
Physics Department, Middle East Technical University
Ankara, Turkey

Muzaffer Atac, Robert Wands, G.P. Yeh
Fermi National Accelerator Laboratory
Batavia, IL 60510 USA

Oleksiy Atramentov, John Hauptman, Jerry Lamsa, Sehwook Lee,
Robert Schoene, Matt Stemper, German Valencia
Department of Physics and Astronomy, Iowa State University
Ames, IA 50011 USA

Michael Gold, John Matthews, John Strologas¹
Department of Physics, University of New Mexico
Albuquerque, NM 87131 USA

Nural Akchurin, Heejong Kim, Sungwon Lee, Mario Spezziga,² Richard Wigmans
Department of Physics, Texas Tech University
Lubbock, TX 79409-3783 USA

26 January 2006
Version 0.3

¹Also at Fermilab

²Also at CERN

Abstract

We describe a general purpose detector for a high energy linear collider that can measure with high precision all the fundamental fermions and bosons of the standard model, and thereby access all known physics processes. The detector consists of four basic subsystems: a thin pixel vertex chamber (PV) being developed at Fermilab for high precision vertex definitions and near-beam occupancy reduction; a Time Projection Chamber (TPC) for robust pattern recognition augmented with silicon strip layers for high precision momentum measurement proposed at Saclay; a high precision multiple-readout fiber calorimeter, complemented with an EM dual-readout crystal calorimeter, for the energy measurement of hadrons, jets, electrons, photons, missing momentum, and the tagging of muons; and, a high precision muon system with drift tubes for track measurement and configured as a dual-solenoid field for the inverse direction bending of muons in an air volume to improve upon the iron-determined 10% limitation on muon momentum resolution. The pixel vertex chamber, TPC and calorimeter are inside the solenoidal magnetic field.

Contents

1	General Description of Concept	4
2	Introduction and Background	6
3	Physics of High Precision Hadronic Calorimetry	11
3.1	Contributions to the resolution	11
3.2	DREAM data	12
3.2.1	π^- and “jets”: Beam data 20 \rightarrow 300 GeV	13
3.2.2	e^- : Beam data 8 \rightarrow 200 GeV	16
3.2.3	μ^- : Beam data 40 \rightarrow 200 GeV	17
3.3	GEANT3 calculations of DREAM module	18
4	Four Detector Subsystems	19
4.1	Thin Pixel Silicon Vertex Chamber (PV)	20
4.2	Time Projection Chamber (TPC)	21
4.2.1	Silicon Strips	23
4.2.2	Vertex Resolution and Momentum Resolution	24
4.3	Multiple Readout Fiber Calorimeter	24
4.3.1	Measuring the neutrons	27
4.3.2	Crystal EM section with dual-readout	27
4.4	Muon Dual-Solenoid	28
5	Calibration and Measurement of j, e, γ, μ and ν	31
5.1	Jets (j)	31
5.1.1	u , d , and s quark jets	32
5.1.2	c and b quark jets	33
5.2	Electrons (e)	33
5.3	Photons (γ)	35
5.4	Muons (μ)	36
5.5	Missing transverse momentum (ν)	38
5.6	Jet “Mass” (optional section)	38
6	Near-Term R&D	38
6.1	Measuring the neutrons: binding energy loss fluctuations	38
6.2	Photoconverters	40
6.3	Manufacture of two ILC-type modules	40
7	Physics Event Analysis DRAFT SECTION	41
7.1	IVCRoot analysis system	41
7.2	Event analysis	41
8	Personnel, Schedule, Time and Cost Estimates	43

1 General Description of Concept

The physics intent is a full detector facility with high precision subsystems that allow highly efficient identification of all particles of the standard model, high precision measurements of the energies and momenta of these particles, and therefore full four-vector reconstruction of physics events. This comprehensive measurement and identification of all partons leaves no corner of physics unseen. As a collider that will complement and complete any possible discoveries or anomalies uncovered at the pp Large Hadron Collider (LHC), the e^+e^- International Linear Collider (ILC) will serve physics by completeness and precision of measurements and all with a minimum of ambiguity both at the single event level and at the physics ensemble level.

We intend to satisfy these criteria with new technologies either recently tested or now under R&D development.

Vertex definition for both track momentum and reconstruction, and for b , c quark and τ lepton tagging, is essential for physics. At the ILC, we require bunch tagging and the suppression of hit occupancies in this sensitive detector only tens of millimeters from the beam. The solution we prefer is the "thin pixel" development now starting at Fermilab (Sec. 4.1). This may be years in development, and we will be eager to contribute to its development, especially for whole-detector slice beam tests.

The calorimeter will be a spatially fine-grained dual-readout fiber augmented with the ability to measure the neutron content of a shower. The dual fibers are scintillation and Čerenkov for separation of hadronic and electromagnetic components of hadronic showers[1]. We expect to surpass the energy resolution of the tested DREAM calorimeter with finer spatial sampling and neutron detection (therefore measurement of fluctuations in binding energy losses) through the time development of the scintillation light or by a third fiber specifically for neutron measurement (Sec. 4.3). The calorimeter modules will have fibers up to their edges, and constructed for sub-millimeter close packing, with signal extraction on the outside so that the calorimeter system will approach full coverage without cracks. We are studying a separate EM section in front of the dual-readout calorimeter consisting of a crystal calorimeter with (again) dual-readout of scintillation and Čerenkov light to provide better photoelectron statistics and to achieve better energy and spatial resolutions for photons and electrons.

The calorimetry will be complemented with excellent tracking by a Time Projection Chamber (TPC). Both the tracking and calorimetry will be very close to 4π coverage, excepting the necessary forward stay-clears for luminosity and beam monitoring, without cracks or holes in the acceptance. The TPC will be a fast drift, moderate magnetic field volume with wire mesh gas electron multiplication detectors on the ends and fast processing electronics for zero-suppression and high level trigger. The TPC volume will be surrounded on its inner and outer radii with high precision silicon strip detectors to improve the momentum resolution.

The muon system will be a dual-solenoid magnetic field configuration in which the flux from the inner solenoid that defines the TPC tracking field is returned through the air-space annulus between this inner solenoid and an outer solenoid with a smaller turn density. The magnetic field in this air volume between the two solenoids will back-bend the muons for a second measurement of the momentum to achieve high precision without the limitation of multiple scattering in Fe , a limitation that fundamentally limits momentum resolution in conventional muon systems to 10%. We can use high spatial precision drift tubes in the air annulus outside the calorimeter, similar to ATLAS, with spatial resolution of $80\mu\text{m}$ per tube.

2 Introduction and Background

The International Linear Collider (ILC) will produce massive quarks (t and b) and massive gauge bosons (W and Z) in precision tests of the Higgs boson hypothesis and further hypotheses on the origin of mass. This is the highest priority in international high energy physics, and the several billion dollar investment in the Large Hadron Collider (LHC) is a measure of that priority. New instruments for the ILC must be capable of measuring all the basic partons of the standard model, including the W and Z in all their decay modes, with a precision and a purity that will be new in high energy physics.

We introduce two new detector ideas in this 4th concept description (triple-readout calorimetry and a new dual-solenoid muon field geometry), and borrow several ideas from other proposals and existing detectors.

New instruments have always led to improved and sometimes important experiments in high energy physics. We have developed a new calorimeter technology that allows high precision measurement of hadronic particles and hadronic jets, and we are designing a new dual-solenoid muon system for high precision measurement of muon momenta after the calorimeter volume. Superior calorimeter performance was achieved with a fiber calorimeter [1], described in Sec. 3, loaded with both scintillating and quartz, or Čerenkov fibers, in which the Čerenkov fibers sampled exclusively the electromagnetic component of each hadronic shower and the scintillating fibers sampled the total charged particle content of each shower. In this way, the electromagnetic (EM) fraction was measured each event[2].

We show the energy resolution of this dual-readout calorimeter for 200 GeV π^- in three stages (Fig. 1); (a) the direct pulse height distribution of the scintillating fibers only, (b) the scintillating (S) and Čerenkov (C) fibers together to correct $e/h = 1$ event-by-event using only the direct S and C signals, and (c) using both scintillating and Čerenkov fibers and, in addition, using the known beam energy in the $e/h = 1$ correction to suppress the leakage fluctuations. These are shown in Fig. 1(a-c), respectively.

The directly measured energy resolution for 200 GeV π^- is

$$\sigma_E/E \approx 14\% \quad (\text{direct, raw scintillation response}),$$

as seen in Fig. 1(a), and which includes fluctuations in electromagnetic fraction and leakage fluctuations. Using only the measured scintillating signal (S) and the Čerenkov signal (C), and correcting each event to $e/h = 1$, the energy resolution improves to

$$\sigma_E/E \approx 5.1\% \quad (\text{called Q/S method in [12]}).$$

This estimate still includes lateral leakage fluctuations of 2-4%. The energy resolution using the known beam energy to perform the $e/h = 1$ correction that effectively suppresses leakage fluctuations is

$$\sigma_E/E \approx 2.2\% \quad (\text{called (Q + S)/E method in [12]}).$$

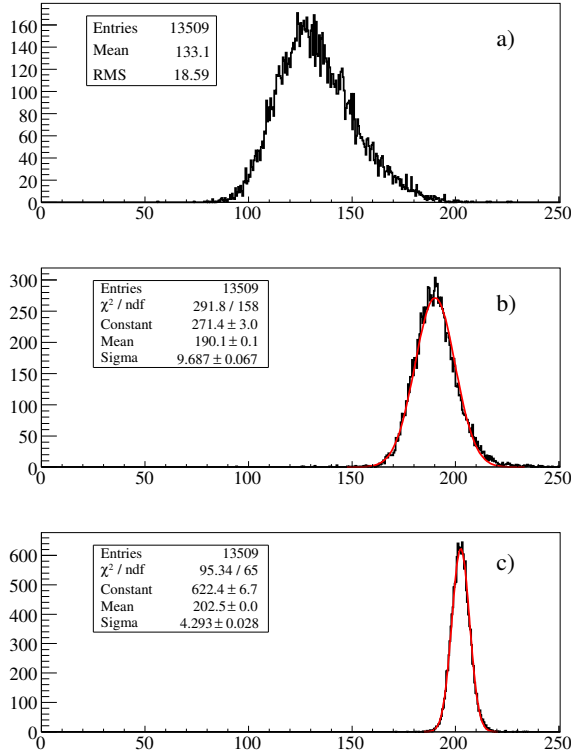


Figure 1: (a) The distribution of the scintillator (S) signal for 200 GeV π^- . This is the raw resolution that a scintillating calorimeter would achieve; (b) the energy distribution corrected to $e/h = 1$ using only the S and C (Čerenkov) signals for each event. This result has leakage fluctuations of approximately 2-4% contributing to the resolution; and, (c) the energy distribution using the known beam energy (=200 GeV) to correct to $e/h = 1$ for each event, thereby suppressing the effects of leakage fluctuations.

Analytically introducing the shower resolution fluctuations for the fixed beam energy results in a resolution of

$$\sigma_E/E \approx 3.2\% \quad (\text{resolution fluctuations introduced analytically}).$$

We do not know experimentally the energy resolution of this dual-readout module in the absence of leakage fluctuations, but presumably it is between 2.2% and 5.1% for π^- at 200 GeV. From fits to the resolution at all energies, this module has a constant term of approximately 2% (see Fig. 8), possibly due to several small effects, all of them controllable[3]. For “interaction jets” these resolutions are about the same, or slightly better.

We do not know the ultimate resolution of this technique, nor of the proposed extensions of this multiple-readout idea, but suspect it will be closer to the lower figures with leakage fluctuations and binding energy loss fluctuations suppressed. This DREAM test module was not intended nor designed to produce the best possible energy resolution, but rather to be a proof-of-principle module for the dual

readout idea. Clearly, the known and expected leakage fluctuations of approximately 2-4% will severely limit energy resolution, but will not too adversely affect the assessment of the dual readout technique.

In reference to the energy distributions in Fig. 1, the beam energy has *not* been used to normalize the means of these distributions. The absolute calibration for the test module was done with 40 GeV e^- directed at the centers of the 19 towers of the module [12], and the subsequent measured hadronic energies are in the same units. The resulting linearity of the hadronic response is shown in Fig. 2 for π^- data from 20 to 300 GeV. The full spread of hadronic response is 3% using the Q/S method, that is, using *only* the Čerenkov (Q) and the scintillation (S) signals for each event.

In addition to hadronic response linearity, the dual-readout calorimeter yields nearly Gaussian response at every energy [12]. These two features are as important to successful calorimetry as raw energy resolution itself.

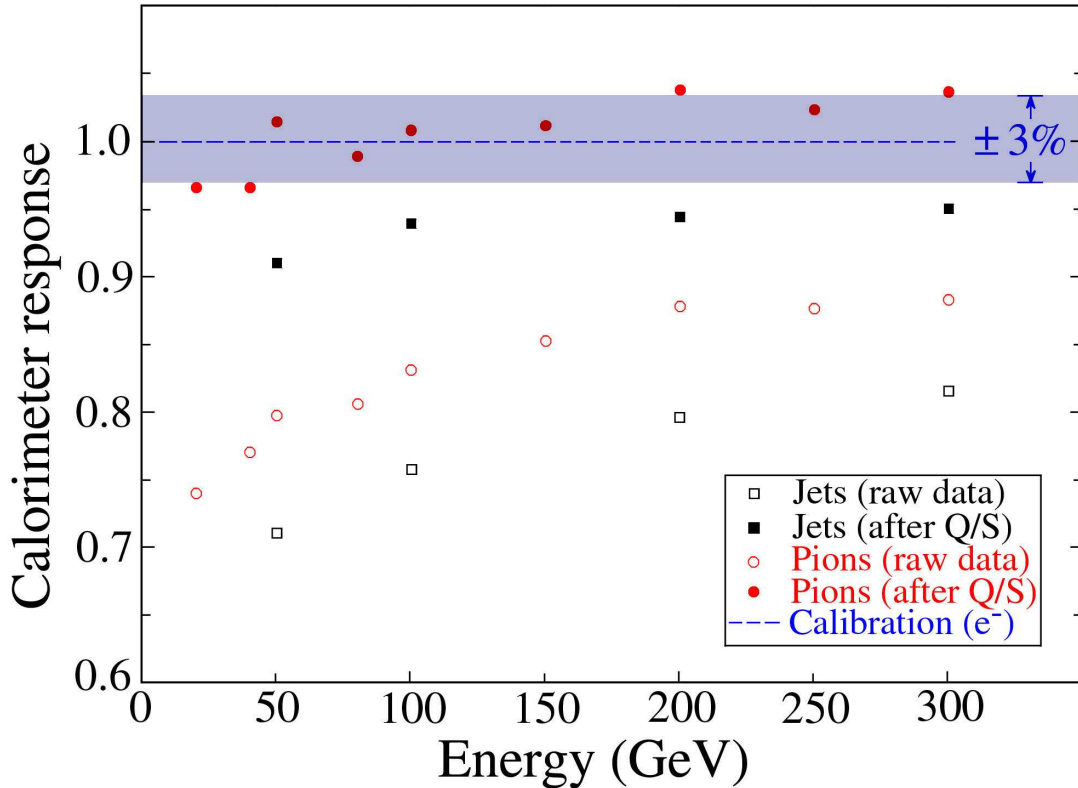


Figure 2: The hadronic response of the DREAM module to π^- and "interaction jets" from 20 to 300 GeV using the Q/S method to correct each event to $e/h = 1$, *i.e.*, using only the Q and S signals each event. See [12] for further details.

In stand-alone particle-level simulations with Pythia, and using the anticipated resolution of this calorimeter of $20\%/\sqrt{E}$, complete with tower granularity and jet reconstruction with LUCCELL, we reconstruct $W \rightarrow jj$ and $Z \rightarrow jj$ decays with a

mass resolution that separates W from Z by better than a Rayleigh criterion, as shown in Fig. 3.

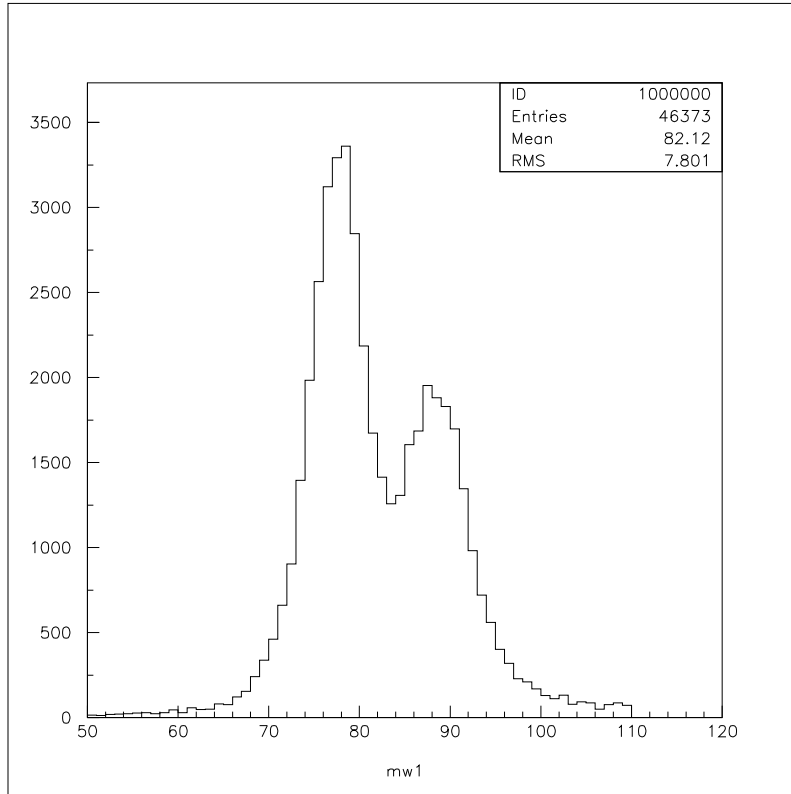


Figure 3: The reconstructed $W \rightarrow jj$ and $Z \rightarrow jj$ mass distribution from Pythia events showered in a DREAM tower calorimeter and reconstructed using LUCCELL.

Therefore, we expect to easily separate $W \rightarrow jj$ from $Z \rightarrow jj$ decays and thereby recover nearly the totality of produced W and Z bosons, excepting only $Z \rightarrow \nu\nu$. More important than event rates, however, is the fact that the W four-vectors are measured without a missing neutrino, and they can be used directly in mass searches, cross sections, angular distributions, *etc.* The W and Z will be like other measured partons in this detector. The excellent energy resolution affords secondary benefits. A 1-prong or 3-prong τ decay is reconstructable kinematically since there is only one unknown: the magnitude of the $\nu(s)$ momentum in the decay, assumed to be aligned with the charged decay products. This is also possible for semi-leptonic c and b quark decays.

The data taken in this proof-of-principle DREAM test module are discussed in Sec. 3.2, and its transformation into an ILC-ready detector is described in Sec. 4.3.

This excellent and spatially detailed calorimetry will be complemented by a Time Projection Chamber (TPC), a comparably excellent and spatially detailed tracking detector with full coverage, for event reconstruction and track definition. These combined detectors will allow high precision energy measurements and event

reconstruction, and also allow powerful quark-gluon separation and background rejection. The potential appearance of new topology events in this detector with such unambiguous three-dimensional tracking and clean, high precision energy measurements will maintain the potential of identifying ‘zoon’ events that may appear in this new energy regime. The TPC is discussed in Sec. 4.2.

The vertex chamber is discussed in Sec. 4.1 and the muon system is discussed in Sec. 4.4. A brief description of how each parton is measured in this facility is given in Sec. 5, and we list further R&D work to be done on this concept in Sec. 6.

3 Physics of High Precision Hadronic Calorimetry

The DREAM calorimeter was designed to explicitly separate the scintillation and Čerenkov light developed in a hadronic shower into physically separate fibers with no ambiguity, and therefore each shower is measured independently twice. In these hadronic showers, there are several physical fluctuations that contribute to the total energy resolution in complicated ways[1]. For a calorimeter with light readout to a photodetector, such as we are suggesting, the several contributions to the resolution are

$$\sigma = \sigma_{\text{trackstat}} \oplus \sigma_{\text{pe}} \oplus \sigma_{f_{\text{EM}}} \oplus \sigma_{\text{leakage}} \oplus \sigma_{\text{BE}},$$

where \oplus denotes a sum in quadrature.

3.1 Contributions to the resolution

These contributions involve several complicated and intrinsically low energy phenomena: nuclear breakup, binding energy losses, ionization energy loss of low energy particles, *etc.* The important ones are:

1. *track statistics*: fluctuations in the number of primary shower particles generated within the calorimeter volume, and fluctuations in the fraction which traverse a fiber;
2. *photoelectrons, pe*: Poisson fluctuations in the number of photoelectrons (*pe*) measured by the photodetector;
3. *electromagnetic fraction, f_{EM}* : fluctuations in the number of $\pi^0 \rightarrow \gamma\gamma$ and $\eta \rightarrow \gamma\gamma$ produced in nuclear interactions, and therefore fluctuations in the fraction of electromagnetic energy in the hadronic shower;
4. *leakage*: fluctuations in the amount of energy that exits the calorimeter volume and is therefore not measured; and,
5. *binding energy, BE*: fluctuations in the nuclear binding energy losses due to nuclear break-up, which appear in the shower volume as free neutrons.

The ultimate energy resolution of a hadronic calorimeter will rely upon reducing each of these fluctuations to its lowest possible level. We propose to deal with each of these terms in the following way:

1. fluctuations in track statistics are best reduced by performing very fine-grained spatial sampling, and this is accomplished by impregnating the calorimeter volume with fine charged particle sensing optical fibers. The efficacy of this method was powerfully demonstrated long ago in the SPACAL calorimeter[4] that achieved an electron energy resolution of $\sim 13\%/\sqrt{E}$ and a hadronic energy resolution of $\sim 30\%/\sqrt{E}$, with constant terms of 1 – 2%;

2. fluctuations in the photoelectron count (pe) at the output of the PMT are best reduced with high light output scintillating fibers, such as those commonly used in scintillating fiber calorimeters today[9] and by using high quantum efficiency photoconverters such as the MultiPhoton Counter (MPC) or other so-called silicon photomultipliers[6, 10].
3. fluctuations in the electromagnetic fraction (f_{em}) are eliminated by the dual-readout technique demonstrated by the DREAM calorimeter module [12], in which an estimated energy resolution of approximately $20\%/\sqrt{E} \oplus 2\%$ when leakage fluctuations are suppressed by using the known beam energy. The efficacy of one additional fiber (a clear fiber of either quartz or plastic) in which Čerenkov light is generated almost exclusively by the electromagnetic particles of the hadronic shower allows us to effectively set $e/h \approx 1$ event-by-event.
4. fluctuations in leakage are only reduced by making a sufficiently large calorimeter medium, and this usually implies $10 \lambda_{int}$ or more in depth and 4-5 λ_{int} in width. So-called tail catchers and gap fillers are only partial solutions to reducing these fluctuations; and,
5. fluctuations in nuclear binding energy losses are best reduced by measuring the neutrons liberated in a hadronic shower, and this can be reasonably accomplished by measuring the MeV-energy recoil protons in a hydrogenous medium in two ways. The first method is to introduce a third fiber, maybe loaded with Li, or with a Birks' constant differing from that of the scintillator fiber, as a means to separately sum the low energy proton ionization signals from $np \rightarrow np$ scatters. The second method is to read out the scintillating fiber in time for 100-200 ns. The early light is from the e, π , and p , and the later light is preferentially from the scattered protons from $np \rightarrow np$, (see Sec. 4.3.1 and Fig. 13), which comes tens to hundreds of nanoseconds later than both the scintillation and Čerenkov light. Therefore, we will study and test the feasibility of all these methods. In the latter case, we would also read out the Čerenkov fibers in time, both as a calibration standard, and as a means of checking and correlating the late light with electromagnetic or hadronic origins, that is, late light not associated with corresponding light in the Čerenkov fibers can be attributed to $np \rightarrow np$ scatters.

Such extreme control of the measurements of space, time and electromagnetic particle content is possibly the very best avenue to achieve excellent hadronic jet energy resolution required for the high precision reconstruction of $W \rightarrow q\bar{q}$ and $Z \rightarrow q\bar{q}$ decays that are the basis of this concept.

3.2 DREAM data

The data taken in the H4 beam in the north area at CERN consist of six million beam triggers on electrons, pions, muons and 'interaction jets' from 8 to 300 GeV.

3.2.1 π^- and “jets”: Beam data 20 \rightarrow 300 GeV

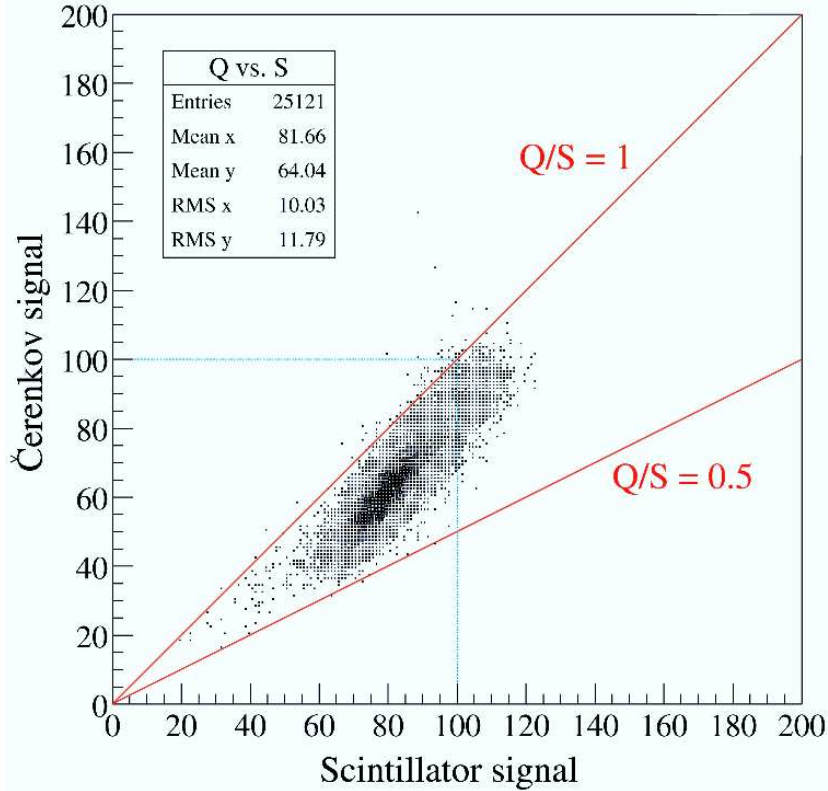


Figure 4: The Čerenkov response of the quartz fibers (Q) *vs.* the response of the scintillation fibers (S) to 100 GeV π^- .

A more complete discussion of the following points is contained in the papers [1, 12]. The dual-readout of Čerenkov and scintillation fibers is shown in Fig. 4 for incident π^- beam at 100 GeV, from which several features are evident:

- the mean energies for both Čerenkov and scintillation fibers are less than the incident beam energy;
- the distributions are not proportional;
- the response to electromagnetic energy is larger than for non-electromagnetic energy;
- the distributions are asymmetric;
- the fluctuations are large, that is, the excursions in the Čerenkov signal, for example, range from 20% to 100%; and,
- the response is non-linear in beam energy (when all energies are studied).

In general, for either Čerenkov or scintillation fibers, the response of a calorimeter to hadronic shower energy deposits has two components: the electromagnetic

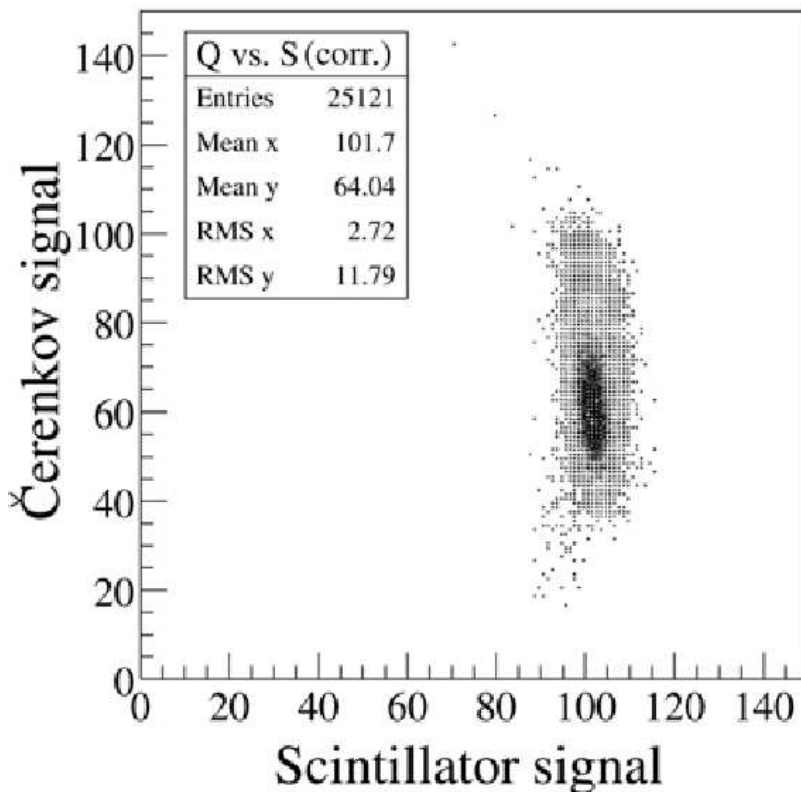


Figure 5: The response of the dual-readout calorimeter after a simple linear correction for the electromagnetic fraction event-by-event for the 100 GeV π^- triggers.

shower particles e^\pm deriving primarily from $\pi^0 \rightarrow \gamma\gamma$ decays, and hadronic particles π^\pm , K^\pm , slow p from nuclear break-up, stopping particles, and μ^\pm from the decays of π and K . In general, the response R to these two components is different, and is grossly represented as the ratio (e/h) which is usually larger than 1, that is, the electromagnetic part (e) produces a larger signal (dE/dx , scintillation light, *etc.*) than the hadronic (h) part. The overall response can be written as

$$R = f_{\text{EM}} + \frac{1}{(e/h)}[1 - f_{\text{EM}}],$$

where the non-electromagnetic part is scaled by (e/h) . Combining this with the sum of the Čerenkov and the scintillation signal, $(S + Q)$, found to be very linear [12] in the electromagnetic shower fraction, f_{EM} , and represented by the linear relation

$$\frac{Q + S}{E_{\text{beam}}} = 0.91 + 1.09f_{\text{EM}},$$

allows us a simple translation of each event in Fig. 4 to extract an excellent estimate of the shower energy. The non-compensating constants (e/h) for Čerenkov and scintillation fibers are about 5 and 1.4, respectively, and depend on the details of the calorimeter such as the medium, fiber fractions, *etc.* This estimate

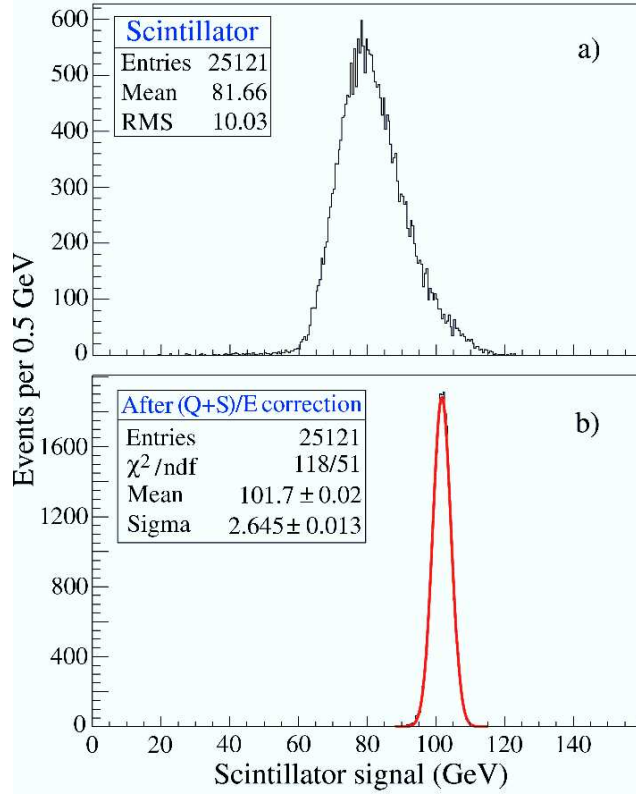


Figure 6: (a) The raw response of the scintillating fibers (S) to a 100 GeV π^- beam; and, (b) the response corrected to $e/h = 1$ using the known beam energy in the correction to suppress the effects of leakage fluctuations, expected to be about 4% in this 1 tonne module. Therefore, the response in (b) is the best that could ever be achieved in a module of this design.

of the shower energy is

$$E = S + 0.453[1.9 \cdot E_{\text{beam}} - (Q + S)],$$

and the distribution of E is shown in Fig. 5. The projection of this distribution is shown in Fig. 6, displaying an energy resolution of 2.6% and a mean calorimeter shower energy very close to 100 GeV in a calorimeter *calibrated only with electrons*. Furthermore, no attempts have been made to embellish this analysis with quadratic terms or even more accurately determined values of (e/h) .

At this level of $\sim 2\%$ there are many systematic and instrumental effects that can only broaden the distribution and degrade the resolution. We have not attended to these effects. Furthermore, as stated earlier, the DREAM module is a proof-of-principle module not intended to achieve the best energy resolution nor to suppress all systematic effects at the 1% level that contribute to the energy resolution and the constant term.

The DREAM module was also exposed to a 'jet' beam generated by high energy π^- interacting in a thin plastic target ($\sim 0.1 \lambda_{\text{int}}$) that resulted in a spray of hadrons

into the calorimeter with nearly the full beam energy and with a small amount of wide-angle energy missing the calorimeter. These we call 'interaction jets', and for purposes of calorimetric assessment, these 'jets' contain all the necessary fluctuations in electromagnetic content, hadron multiplicity, energy spectrum, *etc.*, of QCD jets.

The Čerenkov and scintillation signals from these 'jet' data are subjected to *the same transformation as that used for the single pion data, viz.*, there are no free parameters, yielding the distribution in Fig. 7. The energy resolution for these 200 GeV 'jets' is about 2.1%, comparable to the single π^- resolution.

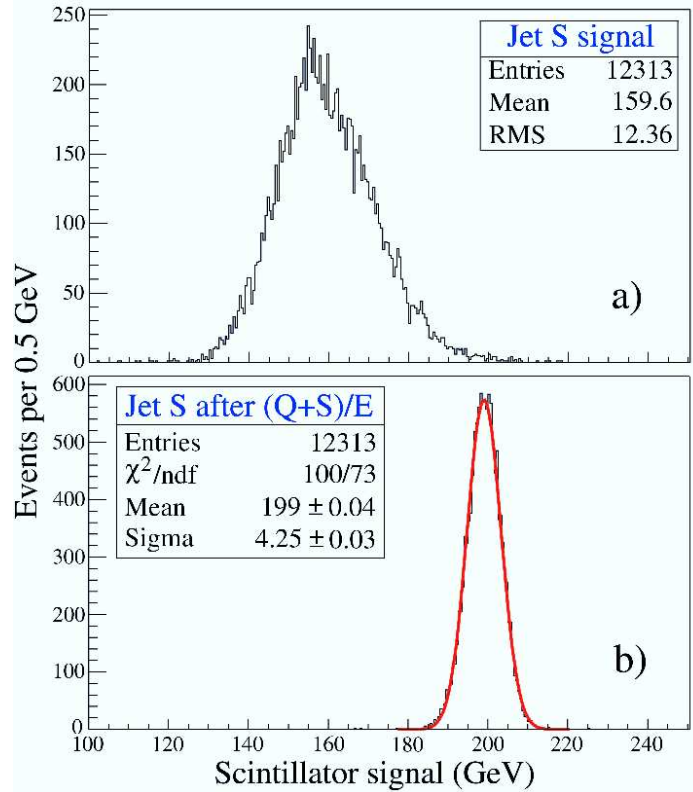


Figure 7: The response of the dual-readout calorimeter after correction for the electromagnetic fraction event-by-event by the same simple linear correction used for pion. These data are for 200 GeV 'interaction jets'.

The energy resolutions for single π^- and 'jets' for all the beam energies shown in Fig. 8. It is clear that this calorimeter technology scales well with \sqrt{E} and with a small constant term.

3.2.2 e^- : Beam data $8 \rightarrow 200$ GeV

Electrons in the DREAM module are very narrow, depositing about 92% of their energy in a single channel. The energy resolution is shown in Fig. 9, in which the scintillating fibers measure a superior energy resolution of $20.5\%/\sqrt{E} + 1.5\%$.

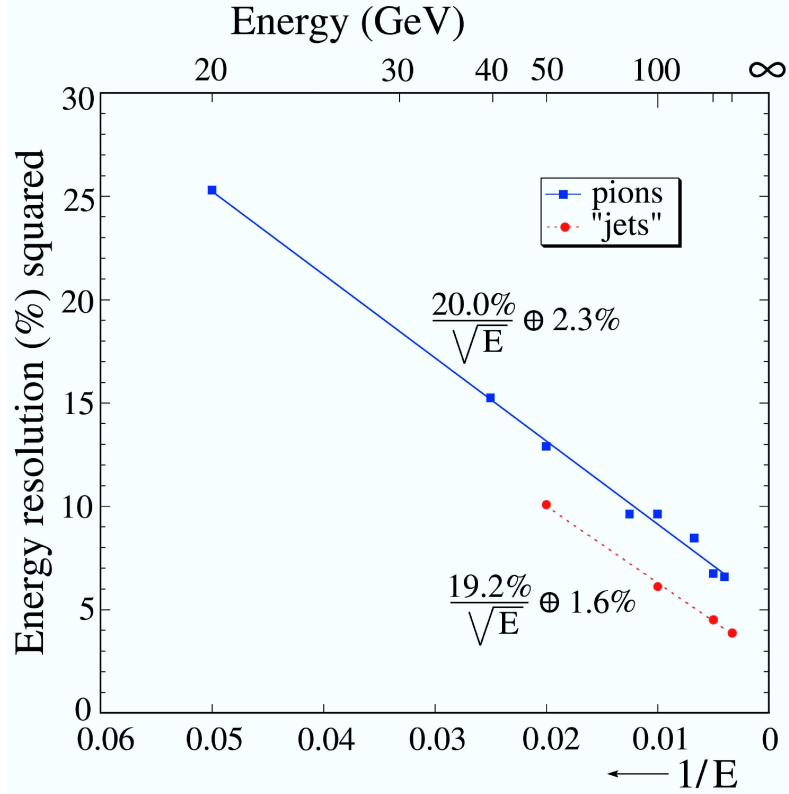


Figure 8: All π^- and 'interaction jet' data taken with the DREAM module showing the nearly perfect scaling of energy resolution in \sqrt{E} .

The Čerenkov measurement is independent and a better estimate could be made by combining these two measurements, but we have not done that.

3.2.3 μ^- : Beam data 40 \rightarrow 200 GeV

The response of the scintillation and Čerenkov fibers to 200 GeV muons is shown in Fig. 10, and the means of these distributions as a function of muon energy are shown in Fig. 11.

For a muon approximately aligned with the fibers, the Čerenkov light emitted at the Čerenkov angle of 45 degrees falls outside the numerical aperture of the fiber, and no Čerenkov light is captured. The radiative processes of bremsstrahlung and pair production by muons generate electromagnetic showers on the interior of the calorimeter that are measured in the same way as incident electron showers. The scintillating fibers measure the sum of the ionization energy loss and the radiative energy loss, whereas the Čerenkov fibers measure only the radiative loss. Therefore, the difference (S-C) is the ionization energy loss, and this difference is about 1 GeV in the two meters of Cu, and independent of muon energy. This can serve as a muon tag.

The DREAM data have demonstrated that a dual readout geometry allows a

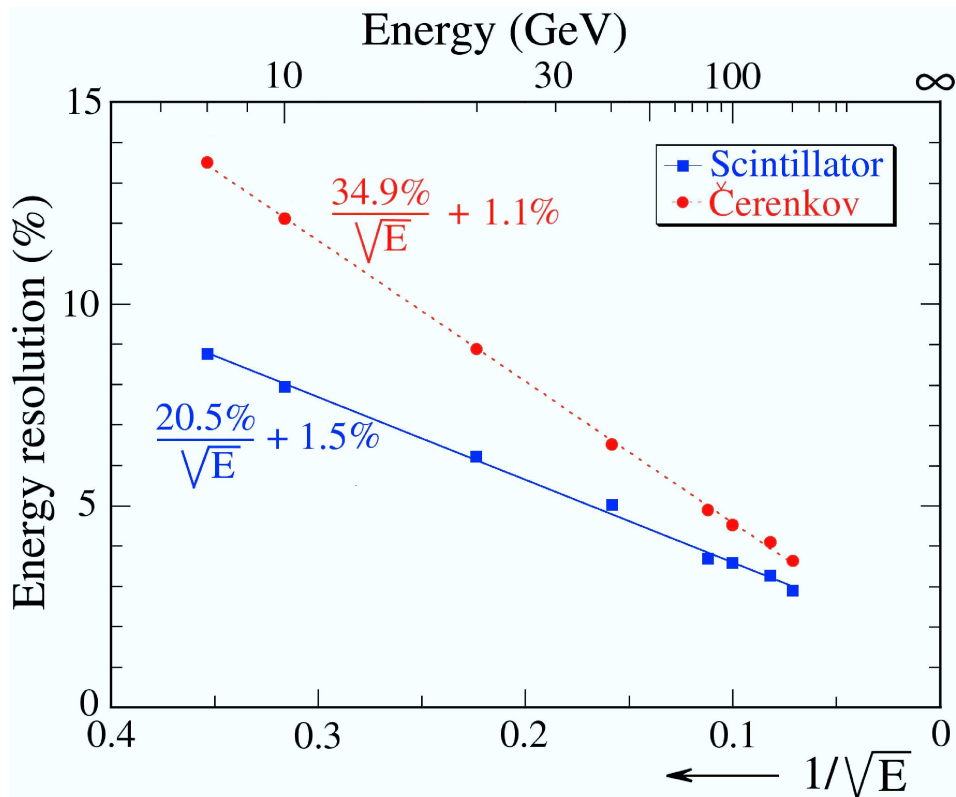


Figure 9: Electron energy resolution for scintillation and Čerenkov fibers, separately. The final energy resolution for electrons can be slightly improved over these separate results by some combination of the scintillation and Čerenkov signals. This has not yet been done.

simultaneous excellent measurement of electron (and photon) showers, a distinctive muon tag, and anticipated excellent hadronic energy resolution on jets, which in turn allows reconstruction of $W \rightarrow jj$ and $Z \rightarrow jj$ decays, and by subtraction a comparably good energy and directional resolution on a missing neutrino four-vector. In addition, the TPC tracking inefficiency is very small, and therefore we measure photons as well as electrons. The muon and electron tagging allows the identification of c and b quark jets, and τ 1-prong and 3-prong decays (85% of τ decays) are reconstructable with only one unknown, the missing momentum along the measured charged τ direction.

These powerful features in *one* detector with *one* uniform geometry lead us to believe that we can measure all the particles of the standard model, u , d , s , c , b , e , μ , τ , γ , W and Z , with comparably good precision.

3.3 GEANT3 calculations of DREAM module

The direct experimental understanding of the DREAM module is augmented by GEANT 3 simulations of details of its performance. Generally the agreement with data is good, and in addition the simulation can reveal detailed differential aspects that are averaged over in the data (such as the summed signal is one channel).

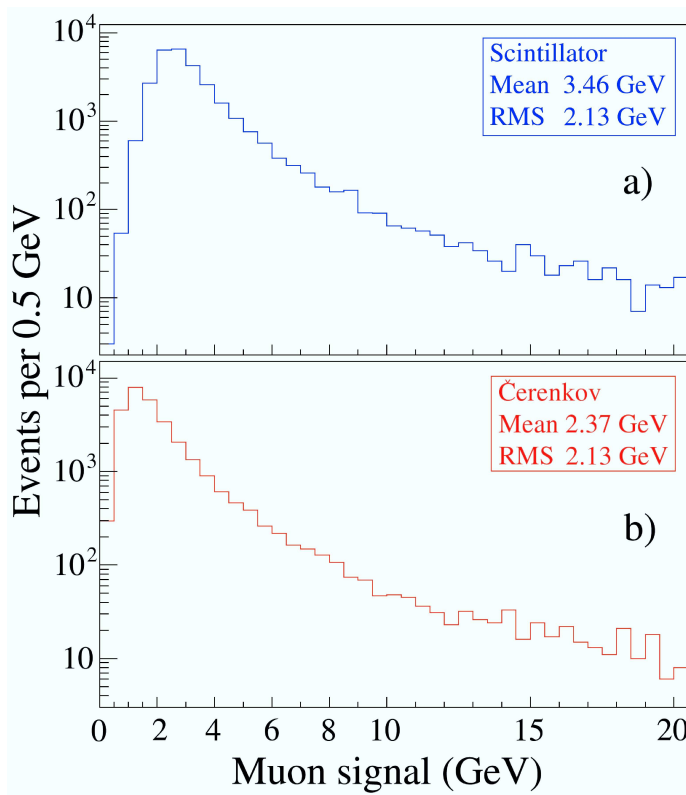


Figure 10: The distributions of Čerenkov and scintillation fiber signals for muon tags in a 200 GeV π^- beam. This distribution is a combination of a Landau dE/dx distribution of energy losses plus the pair production and bremsstrahlung stochastic losses in the absorber.

4 Four Detector Subsystems

In this initial definition of a detector facility at the ILC, we describe four subsystems, arranged in the usual order:

1. a high spatial precision, low mass vertex detector close to the beam, for vertex definition, c and b quark and τ lepton tagging, occupancy suppression, and track definition for momentum resolution. This vertex detector will be a ‘thin pixel’ silicon-based detector [8] with several layers, including axial coverage;
2. a large volume tracking system consisting of a Time Projection Chamber (TPC) for comprehensive pattern recognition in any potentially complicated event environment, complemented with silicon strip $r - \phi$ measurements before and after the TPC for high precision momentum measurement;
3. a multiple readout calorimeter, a further improvement beyond the current dual-readout DREAM test module, for comprehensive energy measurements of electrons, photons, hadrons and jets, including the four-vector reconstruction of W and Z decays to quarks, and the tagging of muons traversing the

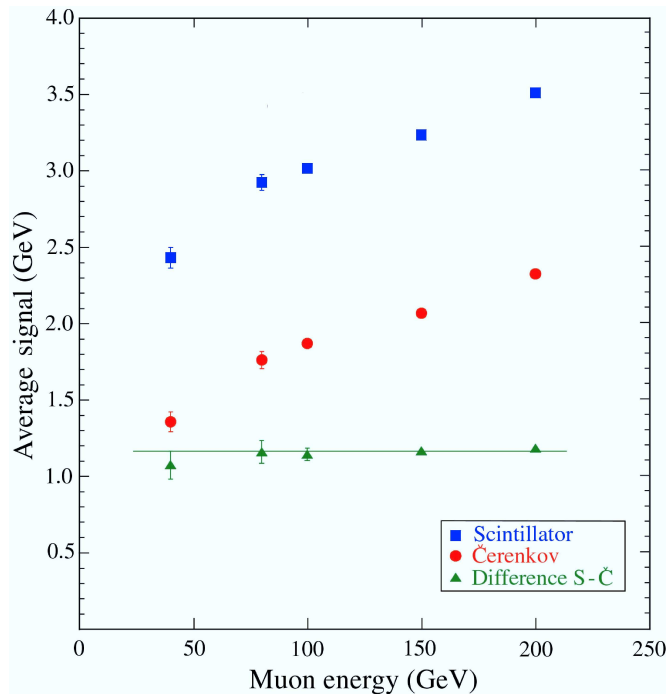


Figure 11: The difference of the scintillation and Čerenkov signals for muon tags in a 200 GeV π^- beam. Since the scintillation fibers measure both ionization energy loss (dE/dx) and radiative energy losses by bremsstrahlung and pair production, while in contrast the Čerenkov fibers measure only the radiative losses, the difference (S-Q) should be nearly a constant equal to the dE/dx of a muon in two meters of Cu, possibly with a Landau tail. We see this constant difference at all muon energies.

calorimeter volume. A crystal EM section, that is also dual-readout, will complement this deeper fiber calorimeter; and,

4. a muon system outside the calorimeter consisting of two solenoids for the reconstruction and momentum measurement in air of tracks exiting from the calorimeter.

4.1 Thin Pixel Silicon Vertex Chamber (PV)

Fermilab is considering the development of thin pixel[8] silicon wafers for high precision spatial tracking for ILC detectors. This generic development will benefit all detectors. The implementation will be conventional in the sense that we desire all the expected features of this new device, including coverage at small angles for overall physics event acceptance.

The design of this thin pixel detector will be challenging. In addition to the spatial resolution, the suppression of hit occupancies in such a critical component of any detector will be important in the new beam environment at the ILC. This

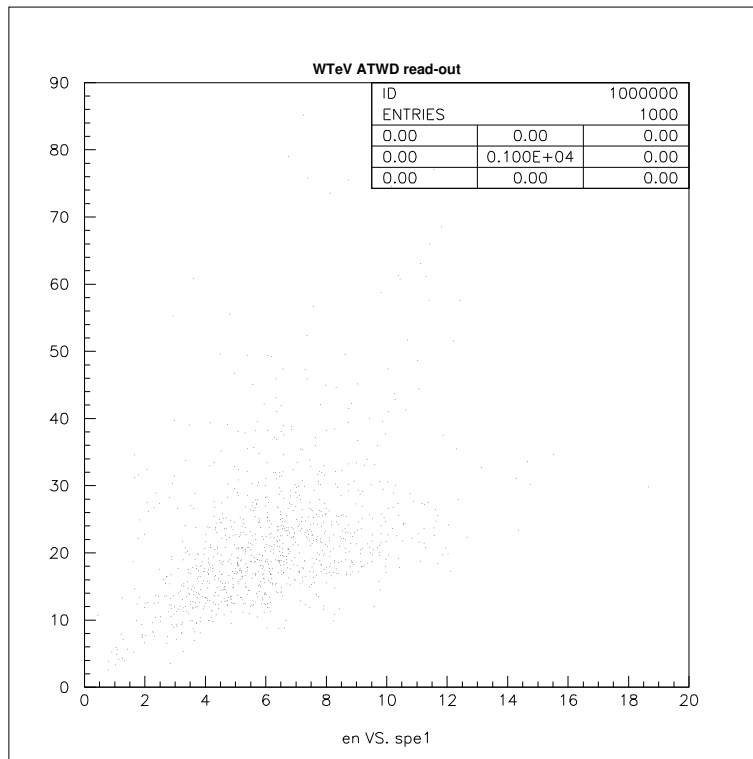


Figure 12: For 100 GeV π^- , the summed neutron kinetic energy at the time of neutron production *vs.* the Scintillator signal in *pe* units summed after 10 ns.

small and fast vertex chamber will also provide the interaction time-tagging for any possible overlapping TPC events.

The pixel vertex detector provides spatial coordinates on charged tracks for momentum measurement when combined with TPC and silicon strip coordinates, and measures the impact parameters of all charged tracks for lifetime tagging of heavy quarks (c, b) and the τ lepton. A impact parameter resolution of $5 \mu\text{m}$ is required for ILC physics, and a pixel size of $5\mu\text{m} \times 5\mu\text{m}$ can achieve this. Multiple scattering and point resolution [5] in a barrel geometry result in an impact parameter resolution of

$$\sigma_b \approx 5\mu\text{m} \oplus 10\mu\text{m}/(p \sin^{3/2} \theta),$$

and therefore both small pixel size and thin silicon are required.

The dimensions of the Fermilab pixel detector as designed for SiD are shown in Fig. 14, and an artistic drawing of its layout around the beam is shown in Fig. 15.

4.2 Time Projection Chamber (TPC)

We believe that a one-atmosphere TPC with micro-mesh or GEM readout [19] in a moderate magnetic field and with a high electron drift velocity will serve well

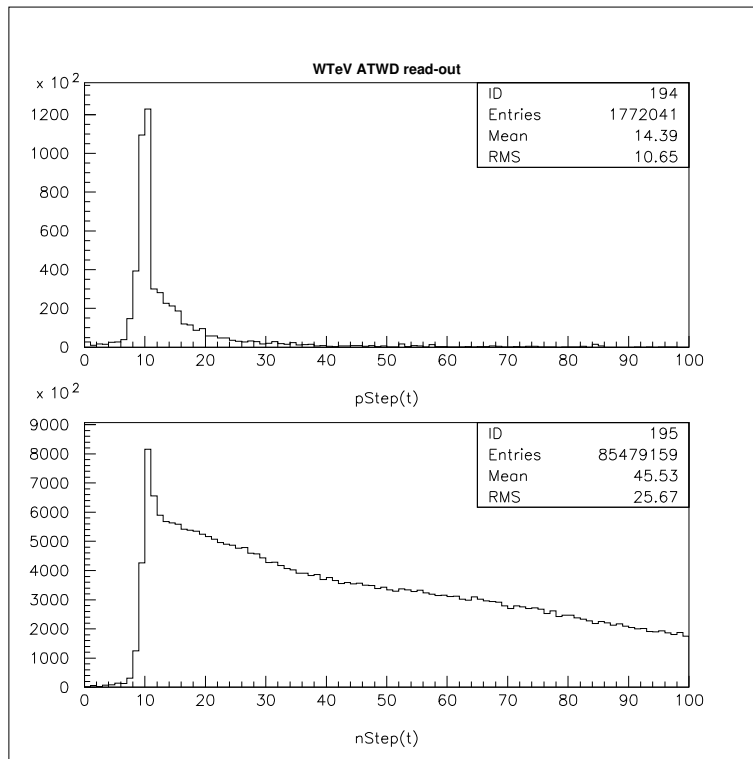
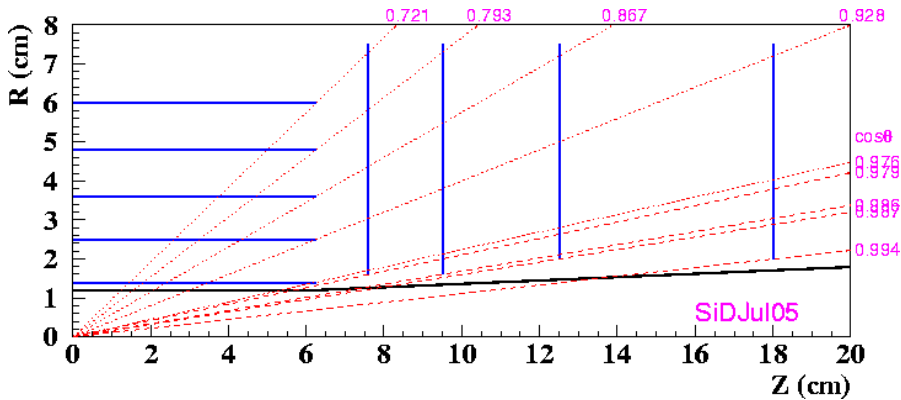


Figure 13: For 100 GeV π^- into the DREAM module, (a) the time distribution of the proton path length; and, (b) the time distribution of the neutron path length. This is a GEANT3 calculation in which the hadronic interactions, and in particular neutron production, are not necessarily correctly done. However, the gross kinematics that are important for this estimate are accurate enough.

for the reconstruction and pattern recognition of tracks in any complicated event. It will serve to define the charged track content of jets, possibly tag quark charge, and be an equal partner with the pixel vertex detector in track reconstruction for multiple interaction vertices and to complement the calibration of the calorimeter with electrons, primarily by tagging and measuring the momenta of electrons from $W \rightarrow e\nu$ decays. At high momenta, the calorimeter resolution will exceed the momentum resolution of the tracking system and we will rely upon $Z \rightarrow jj$ and $Z \rightarrow ee$ decays for calibration.

In the new experimental physics regime of a TeV e^+e^- collider, a three-dimensional imaging tracking detector such as a TPC is essential. The low mass it presents to passing particles, its two-track discrimination and spatial precision are ideal for observing long-lived ($\gamma\beta c\tau \approx 1\text{-}100$ cm) decaying states; its essentially complete solid angular coverage contributes to complete physics events; its measurement of ionization allows searches for free quarks at $1/9$ or $4/9$ ionization, for magnetic monopoles, and for any other exotically ionizing tracks. In addition, the multiple measurements of the z -coordinates along the trajectory of a track yield a measurement of magnetic charge (m) by $\mathbf{F} = m\mathbf{B}$ bending.



1

Figure 14: Schematic of the Fermilab pixel vertex layout. Pixel sizes are anticipated to be about $5\mu\text{m}$. The first layer is as close to the beam as the MDI group will allow, about 1.5 cm, with five layers out to a radius of 6 cm. The usual geometry of axial disks, in this design four disks out to a z coordinate of about 20 cm. Clearly, if these pixel detectors are not too expensive, expanding this array would be very advantageous of any detector.

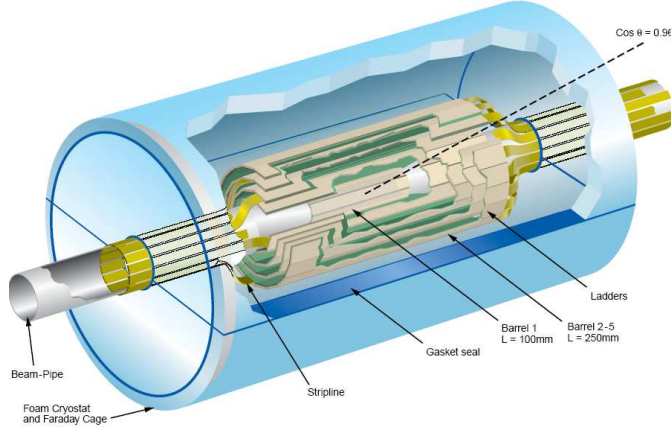
Finally, the dE/dx ionization measurement of a TPC will assist physics analyses involving electron identification, discrimination of singly ionizing e^- from a doubly ionizing $\gamma \rightarrow e^+e^-$ conversion for aligned tracks, and other track backgrounds.

Several groups are designing TPCs for the ILC [20] and we anticipate participating in these designs.

The TPC requires parallel electric and magnetic fields for suppression of transverse electron diffusion and avoidance of $\mathbf{E} \times \mathbf{B}$ drift. A large solenoid outside the calorimeter can provide a sufficient magnetic field.

4.2.1 Silicon Strips

Savoy-Navaro[21] has combined the excellent features of a TPC with the excellent spatial resolution of a silicon strip tracking system. The combination of pixels and silicon strips before the TPC, the large number of track measurements inside the TPC, and silicon strips just outside the TPC is a formidable tracking system that we have not adequately studied. The arrangement of spatial measurements is not the Gluckstern [5] optimum, but maybe as close as possible. Extending the thin pixel



2

Figure 15: An artist's view of the pixel vertex around the beam pipe.

detector to larger radii, pushing the inner TPC radius to larger radius, and using the pixel detector and the beam constraint in the momentum measurement along with an outer Si strip layer outside the TPC is a further possibility. Nevertheless, the weakness of a TPC for a Linear Collider is the moderate momentum resolution for high momentum tracks, and these are possible solutions to that problem.

4.2.2 Vertex Resolution and Momentum Resolution

A vertex impact parameter resolution in x , y and z will be excellent in the thin pixel detector, about several microns, and defines the beginning point of the calorimeter measured jets, while the TPC defines the charged particles that constitute the jet. For N measurements in the TPC of precision σ_0 , and a vertex constraint, the momentum resolution is

$$\sigma_p/p^2 = \frac{\sigma_0}{0.3BL^2} \sqrt{\frac{320}{N+4}},$$

and for $\sigma_0 \approx 100\mu\text{m}$, $\sigma_p/p^2 \approx 10^{-4} (\text{GeV}/c)^{-1}$.

4.3 Multiple Readout Fiber Calorimeter

The motivation for this detector concept is the successful DREAM module built at TTU and tested at CERN, from which five publications have resulted.[12, 14, 15,

16, 17]. The calorimetric measurement of hadronic particles has been bedeviled for decades by

1. poor energy resolution, typically $80 - 120\%/\sqrt{E}$ for big detectors. There are a few exceptions, such as ZEUS at DESY, but $e/h \approx 1$, thereby fixing the senser-absorber ratio;
2. non-Gaussian response. Usually, a high-side tail is a characteristic of hadron calorimeters;
3. non-linearity with energy. The calorimeter response is not linear with incident particle energy.

These serious deficiencies are generally understood[1] to be due to several factors: (*i*) to a non-equal response to electromagnetic and hadronic shower energy deposits (" $e/h \neq 1$ "), (*ii*) the fall-off of calorimeter response to lower energy hadrons in the few-GeV region, (*iii*) the huge fluctuations in electromagnetic energy fraction from shower-to-shower, and (*iv*) variation of the mean electromagnetic shower fraction with increasing hadron energy. These phenomena affect the above list of problems in different ways.

This dual-readout calorimeter has the following main features, as can be seen in the several publications:

1. the energy resolution is expected to be excellent, about $20 - 25\%/\sqrt{E}$ for π 's and "jets" in a module with negligible leakage fluctuations;
2. the response is Gaussian, to a good approximation (Figs. 6, 7); and,
3. the response is linear in hadronic beam energy (Fig. 2).

Most importantly, these exceedingly beneficial features, and in particular the linearity with energy, are obtained *in a calorimeter calibrated with electrons*. The calorimeter we propose for the ILC will be an augmentation and improvement over the present tested proof-of-principle DREAM module [1]. The following items are under consideration, and represent the character of the improvements we expect to make:

1. each fiber will be inserted into its own groove; this will increase the statistical resolution over the DREAM module by reducing the correlation in multiple fiber signals (both scintillating and Čerenkov) arising from the passage of a single track;
2. construct the absorber matrix of tungsten (W). This will reduce the effects of light attenuation in the scintillating fibers, allow a more compact detector to lower the costs of the solenoids and the muon system, and improve slightly the jet and e, γ separation and reconstruction. The next better option is brass;

3. slightly increase the fiber spatial density to account for the smaller Moliere radius of electromagnetic showers in W and the smaller interaction length of hadronic showers;
4. readout both the scintillating fibers and the Čerenkov fibers in time, out to about 500 ns, to catch the slow neutrons whose energy is roughly proportional to the binding energy (BE) losses in nuclei in hadronic showers. These neutrons are approximately $T \sim 1$ MeV, and their velocity is $v \approx \sqrt{2T/M_n} \approx 0.05c$. For a mean neutron interaction length of several centimeters, the expanding neutron content produced by a showering jet will fill possibly 0.5 m^3 over a few hundred ns;
5. in addition to the above item, we will test a third fiber as a specifically neutron sensing fiber, loaded with either Li or B;
6. the geometry of individual modules could be a hexagonal pyramid with the top chopped off (a "truncated hexagon"). This geometry provides a mosaic without cracks between modules, and allows for hexagonal shaped channels that are better suited to showers than square channels. Note that the DREAM module has hexagonal channels. However, this may not be easily compatible with a cylindrical geometry of the tracker and coil, so we also consider a truncated pyramid geometry;
7. use a photoconverter with both higher quantum efficiency (QE), a smaller photosensitive surface to reduce the probability of a direct hit of a particle on the sensitive area of the photoconverter, and that is not sensitive to a magnetic field. This could be the new MultiPhoton Counter (MPC) or another variation of the Silicon Photomultiplier[10]; and,
8. shorten the fiber lengths at the rear of the calorimeter modules to reduce light generated by particles traversing the fibers behind the module.

These multiple-fiber hex geometry calorimeter modules with light readout at the back are perfectly suited for a zero-crack and zero-dead volume calorimeter. Fibers can be in grooves at 1mm from the edge of a module, and therefore be positioned without dead space to an adjacent module. The volume fiber density can be kept constant across the boundaries between modules.

We are studying the design of a crystal EM section in front of this multiple-readout calorimeter, that itself will be dual-readout, to achieve two improvements: an increase in photoelectron statistics for electromagnetic showers, and a better spatial resolution for photons. This is the subject of the LCRD proposal[10].

We propose to build two modules that are essentially final ILC modules (ILC-type) with the above improvements over the proof-of-principle DREAM module, and test it at Fermilab[7].

Cautions (a) W produces more n than brass, and therefore the n measurements become more critical; (b) W is expensive and difficult to machine; (c) if the truncated hexagon is too complicated from a mechanical point of view, we could use a "truncated square pyramid".

4.3.1 Measuring the neutrons

The correlation between the kinetic energy of the neutrons produced in a 100 GeV π^- hadronic shower in DREAM, and the $np \rightarrow np$ signal seen in the scintillating fibers, is shown in Fig. 12, and although this correlation is not exact, it is good enough that we claim to measure the binding energy losses by measuring the MeV neutrons. These issues are addressed in more detail in Sec. 6.

Time History Readout The time distribution of the proton pathlength in the scintillating fibers is shown in Fig. 13 (upper frame) and the time distribution of the neutron pathlength is shown in the lower frame, for 100 GeV π^- showers. The units are nanoseconds. We will further calculate and expect to test this time history readout as a means of measuring the MeV neutrons.

We will also readout the Čerenkov fibers just like the scintillating fibers, in which we expect to see zero signal from neutrons since the scattered protons are far below Čerenkov threshold. The Čerenkov time history will serve several purposes: tag electromagnetic late light not due to neutrons, tag energy deposits from overlapping events, monitor the calorimeter for energetic activity between beam crossings, and serve as a calibration monitor.

Third Fiber There are at least three types of fiber to facilitate the measurement of neutrons: (a) a neutron sensitive fiber loaded with Li or B; (b) a second scintillating fiber with a Birks' constant different from the first scintillating fiber; and, (c) a non-hydrogenous fiber as the scintillator fiber and a hydrogenous fiber for the neutrons.

4.3.2 Crystal EM section with dual-readout

Our LCRD proposal [10] addresses the issue of electromagnetic (e, γ) energy and spatial resolutions critical to ILC physics. The DREAM module had an electromagnetic resolution of $\sigma_E/E = 20\%/\sqrt{E}$ limited by photoelectron (pe) statistics. The point of the LCRD proposal is twofold: (i) consider other photoconverters, such as the Multi Pixel Photon Counter (MPC), and (ii) study a crystal front EM section before the triple-readout hadronic calorimeter that is more finely laterally segmented, has much higher pe yield, and that is also dual-readout (scintillation and Čerenkov). This solution will lead to excellent EM resolutions. The main issue is compatibility with the fiber triple-readout hadronic calorimeter.

4.4 Muon Dual-Solenoid

We introduce two new ideas for the identification and measurement of muons.

1. The dual readout calorimeter uniquely tags a muon by the difference between the scintillation and Čerenkov signals; and,
2. A dual-solenoid allows high momentum resolution on muons bending in an air (or, He) volume.

1. The Čerenkov and scintillation signal distributions for 200 GeV μ^- are shown in Fig. 10. The scintillation signal is the sum of the μ ionization energy loss and the radiative energy loss due to μ bremsstrahlung in the Cu. The Čerenkov signal is due *only* to the radiative energy loss since the μ , mostly aligned with the fibers, produces Čerenkov light that is outside the numerical aperture of the fiber. This is the first time that the separate ionization and radiative components of μ energy loss have been directly measured.

A consequence of this fact is that we can use the difference of the scintillation and Čerenkov signals as a tag for an aligned muon traversal of the calorimeter. Fig. 11 displays the average signal in the scintillating and Čerenkov fibers as a function of μ energy. The difference, $S - C$, is plotted and seen to be flat, *i.e.*, the difference is just the ionization energy loss of about 1 GeV in 2 meters of Cu.

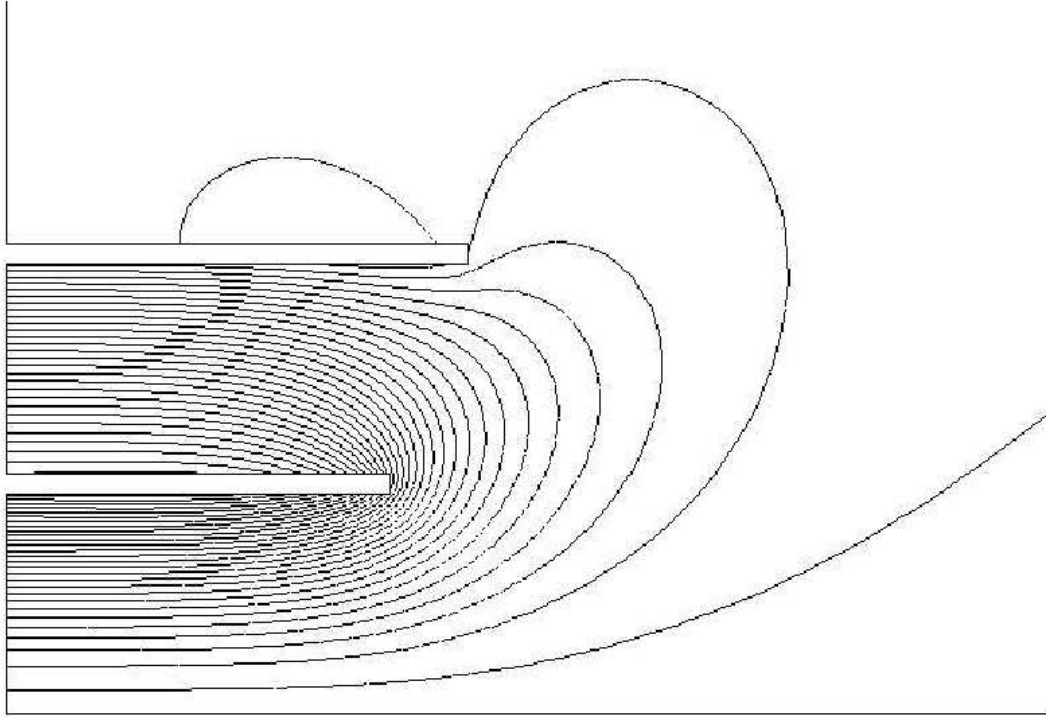
2. The momentum resolution of an Fe-based muon system, in which the magnetic field in the Fe is used to bend the muon trajectory, is limited to 10% by multiple scattering. The ATLAS collaboration has installed magnetic toroids to bend the muons in air, however, to achieve the necessary resolution requires extreme alignment of the toroids over large distances.

Dual-solenoids with inner solenoid just outside the calorimeter providing the uniform tracking magnetic field, and a second larger solenoid outside this solenoid to return the flux, provides a large region of field in air for the bending and momentum measurement of muons that exit the calorimeter. A very simple calculation with two simple solenoids is shown in Fig. 16. We will optimize this field configuration.

These superconducting dual solenoids are easy to align, relatively easy to build, and with nT monitors, can be shimmed into the optimum position. The integral of the field in Tm is about one-half the ATLAS integral but more uniform in polar angle, and this is sufficient for us.

High spatial precision tracking chambers of the KLOE-type may be used in the muon annulus region.

The momentum resolution depends on the field integral along the flight path of a muon, and this is shown in Fig. 17(b) in units of [T·m]. The coil dimensions, currents and turn densities for this example plot are $R_1 = 3\text{m}$, $L_1 = 5\text{m}$, and $i = 15\text{kA}$ with 4 layers of 100 turns per meter. The outer coil has $R_2 = 6\text{m}$, $L_2 = 8\text{m}$, and $i = -7.5\text{kA}$ with the same turn density. The turn density was quadratically increased at the ends of the solenoids by +15% for the inner solenoid,



Flux plot

Figure 16: Magnetic field lines of dual solenoids. The flux density is about 2T in the inner solenoid, and about 1.5T between the solenoids. This field configuration will be optimized to make the inner (tracking) field uniform and to reduce the stray field.

and -15% for the outer solenoid, in order to achieve a uniform B_z in the central $\pm 2\text{m}$ tracking volume.

This integral is larger enough, about 1.5-2.5 T·m, exactly smooth in azimuth angle ϕ , and also smooth in polar angle θ out to $\cos(\theta) \approx 0.85$. The average value of the magnetic field is shown in Fig. 17(a) along the trajectory of a muon from the origin. A typical momentum resolution is about

$$\sigma_{p_\mu}/p_\mu^4 \approx 10^{-4} \text{ (GeV/c)}^{-1}.$$

Momentum resolution depends only weakly on R_2 , the radius of the outer solenoid, since flux density in the inner solenoid $B_1 = W/\pi R_1^2$ (Webers/ m^2) has W Webers that go through the outer solenoid resulting in $B_2 \approx W/\pi(R_2^2 - R_1^2) \sim W/\pi R_2^2$. Increasing R_2 increases the track length $L = R_2 - R_1$ and reduces $B_2 \sim 1/R_2^2 \sim 1/L^2$ so that $B_2 L^2 \sim \text{constant}$.

A muon is therefore measured and identified by all four systems: pixel vertex, tracking (\vec{p}), calorimeter (ID and EM energy), and muon system (\vec{p} and ID).

End cap region The end cap regions are poorly suited for measuring muons with the dual solenoid field alone, however, we are calculating two options: (a) ATLAS-

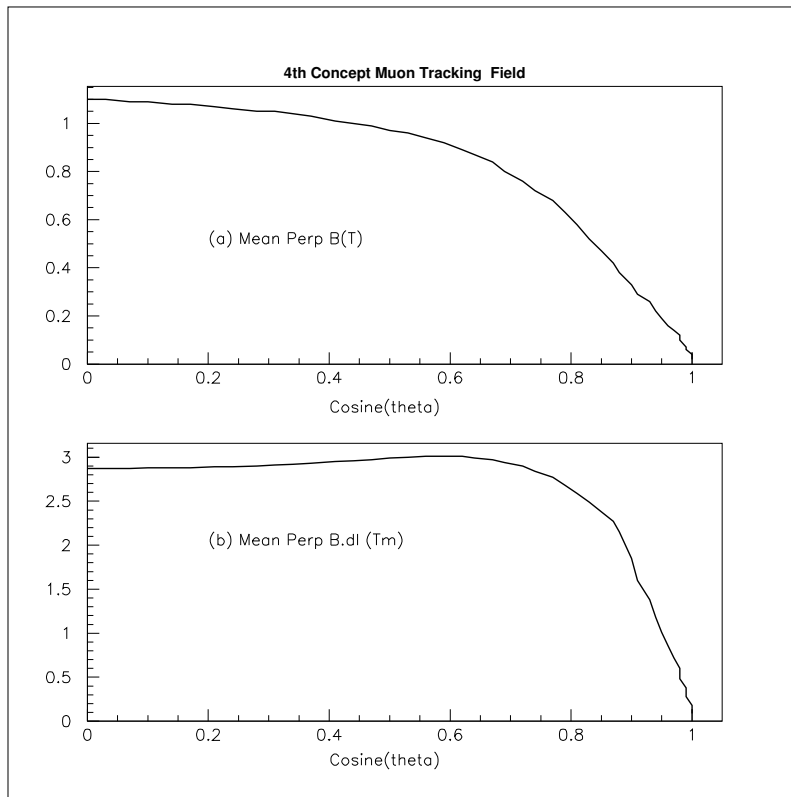


Figure 17: (a) The average value of the magnetic field along the muon trajectory, in T; and, (b) the integral of the field along the muon trajectory, in T·m. This solenoids of this example field are described in the text.

like end-cap toroids, and (b) a wall of circular currents to “close off” the field, drive the field lines out radially, and essentially confine the field to a “tin can”.

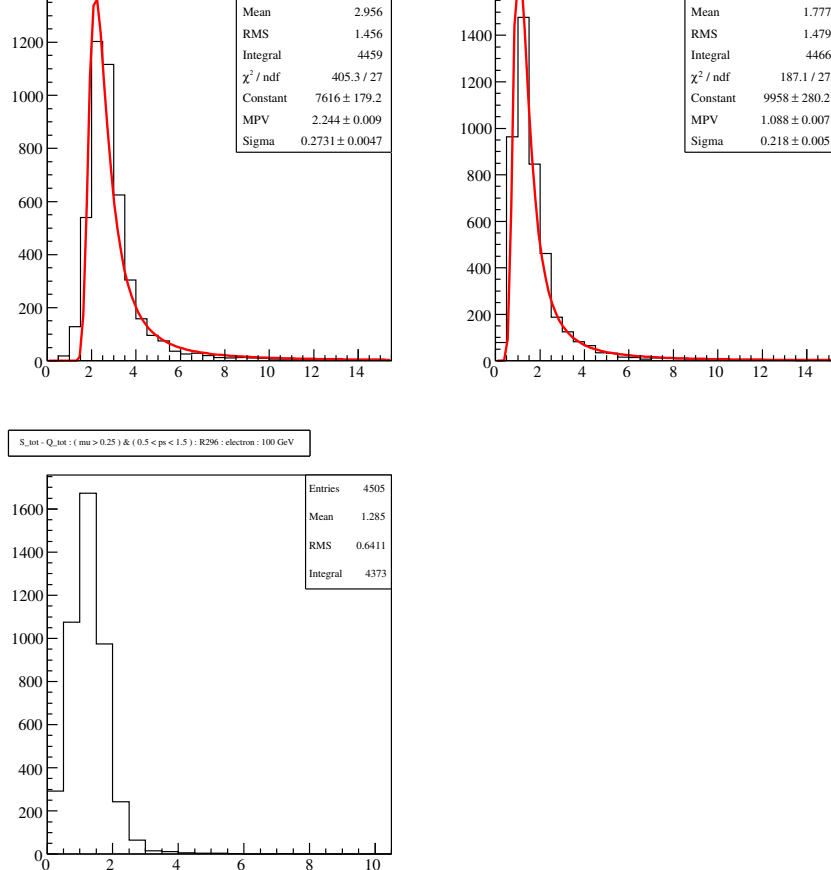


Figure 18: For muons at 100 GeV, (a) the distribution of the scintillating signal, S ; (b) the distribution of the Čerenkov signal; and, (c) the distribution of the difference, $(S - \check{C})$. In this difference distribution, the high-side 1% level is about 3 GeV, and the 0.1% level is about 5 GeV.

5 Calibration and Measurement of j , e , γ , μ and ν

The main goal of this detector is full four-vector reconstruction of all partons. The energy units are defined by the response of the calorimeter to electrons, and these units are used for jets and muons. We have found that this dual readout calorimeter, designed to test for excellent energy measurement of hadronic showers, is also excellent for the energy resolution of electrons, excellent for the identification of electrons due to their spatially narrow signature, and also provides a unique identification signature for a through-going muon, even in the presence of energetic bremsstrahlung or pair production within the calorimeter volume. . Since a missing neutrino is tagged by the missing momentum vector in the event, the precision of this vector is known nearly as well as the jets of the event. A dual-readout crystal electromagnetic section in front of a multiple-readout calorimeter is under consideration[10]. A more precised definition of photons is possible, and this will be tested.

5.1 Jets (j)

Half the fermions of the standard model are quarks and these will be produced copiously at the ILC. The interplay of the decays of massive bosons and the heavy quarks, in addition to the critical study of Higgs and their coupling strengths to the masses of fermions and bosons, and therefore the separate identification and

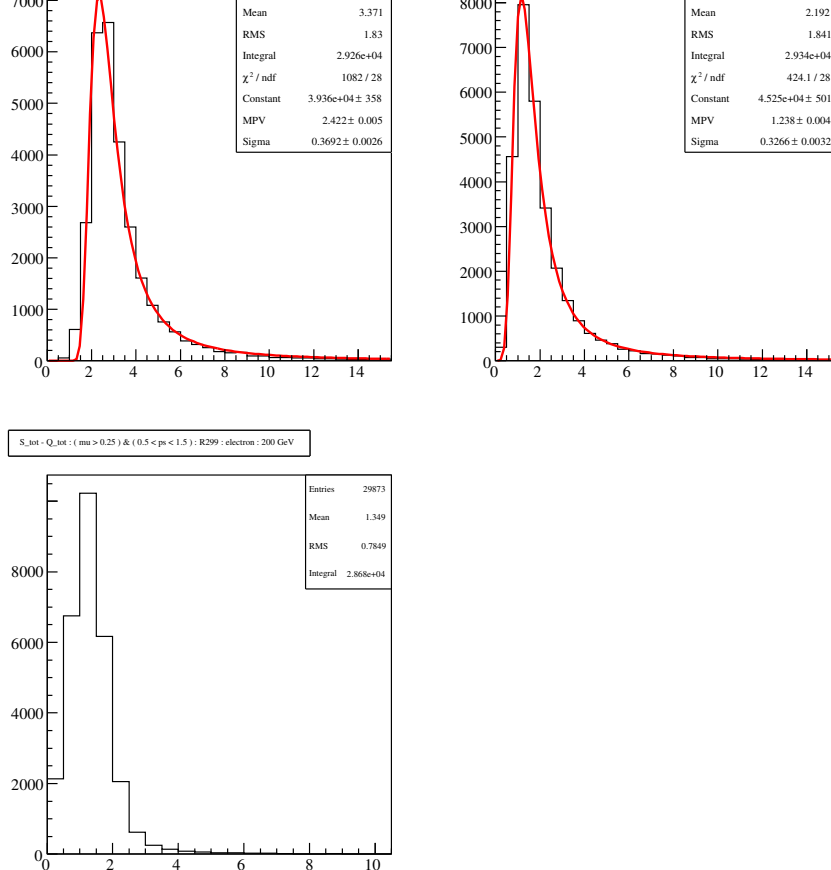


Figure 19: For muons at 200 GeV, (a) the distribution of the scintillating signal, S ; (b) the distribution of the Čerenkov signal; and, (c) the distribution of the difference, $(S - \check{C})$. The 1% level is about 3 GeV, and the 0.1% level is about 5 GeV, very similar to 100 GeV.

accurate reconstruction of individual jets is exceedingly critical for ILC physics.

In this section, we discuss the experimental resolution on jets and pions. See [12] for details.

5.1.1 u , d , and s quark jets

The light quarks are measured with a combination of three systems: the tracking detectors, PV and TPC, and the calorimeter. The calibration of the calorimeter for the energy measurements of jets is crucial. To measure the jet four-vector, we must also measure the vertex point and make a measurement of the jet centroid in the calorimeter.

This dual-readout calorimeter results in a linear response to hadronic energy in a calorimeter *calibrated only with electrons*. Therefore, the approximately 2% jet energy resolution can be maintained in this experiment from the $W \rightarrow jj$, $Z \rightarrow jj$ and $Z \rightarrow ee$ calibration points up to hundreds of GeV.

One critical design problem for 4th is the magnitude of the tracking magnetic field: too low, and momentum resolution suffers; too high, and jet calorimeter pattern recognition suffers. In the DREAM test module exposed to “interaction jets”, a 7.2-cm wide hexagonal channel typically contained 50% of the jet energy, a good number for robust pattern recognition. If the jet products are spread out in azimuth ϕ over several channels, we lose this strength.

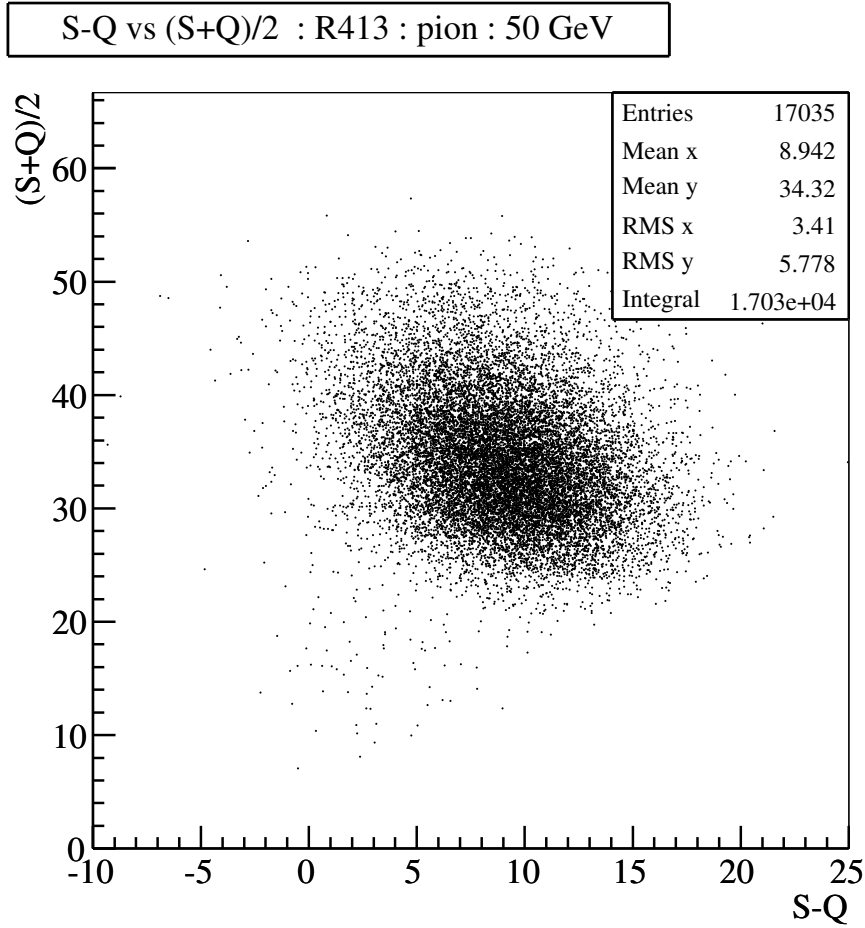


Figure 20: For 50 GeV pions, the distribution of $(S+\check{C})/2$ vs. $(S-\check{C})$ shows 10 events in the muon acceptance region, $0 < (S+\check{C})/2 < E_\mu/4$ and $-1 \text{ GeV} < (S-\check{C}) < 5 \text{ GeV}$, for a pion-to-fake-muon rate of $\sim 10/17K \sim 0.6 \cdot 10^{-3}$.

5.1.2 c and b quark jets

The heavy quark jets are measured with a combination of all detectors: PV, TPC, calorimeter, and muon systems. These quarks can be tagged by a combination of jet invariant mass, e and μ lepton tags, non-zero impact parameter, and missing momentum along the jet axis for jets with missing ν s..

5.2 Electrons (e)

Electrons are measured with a combination of tracking and calorimeter. The best calibration standard for electrons is a sample of $Z \rightarrow ee$ decays. We have tested the response of the dual readout calorimeter to electrons from 8 to 200 GeV, and find an energy resolution of about $20\%/\sqrt{E}$, about the same as for jets, shown in Fig. 9. This is surprising since the electromagnetic resolution should be the limiting resolution for hadrons. However, only one-half of the fibers (the S fibers)

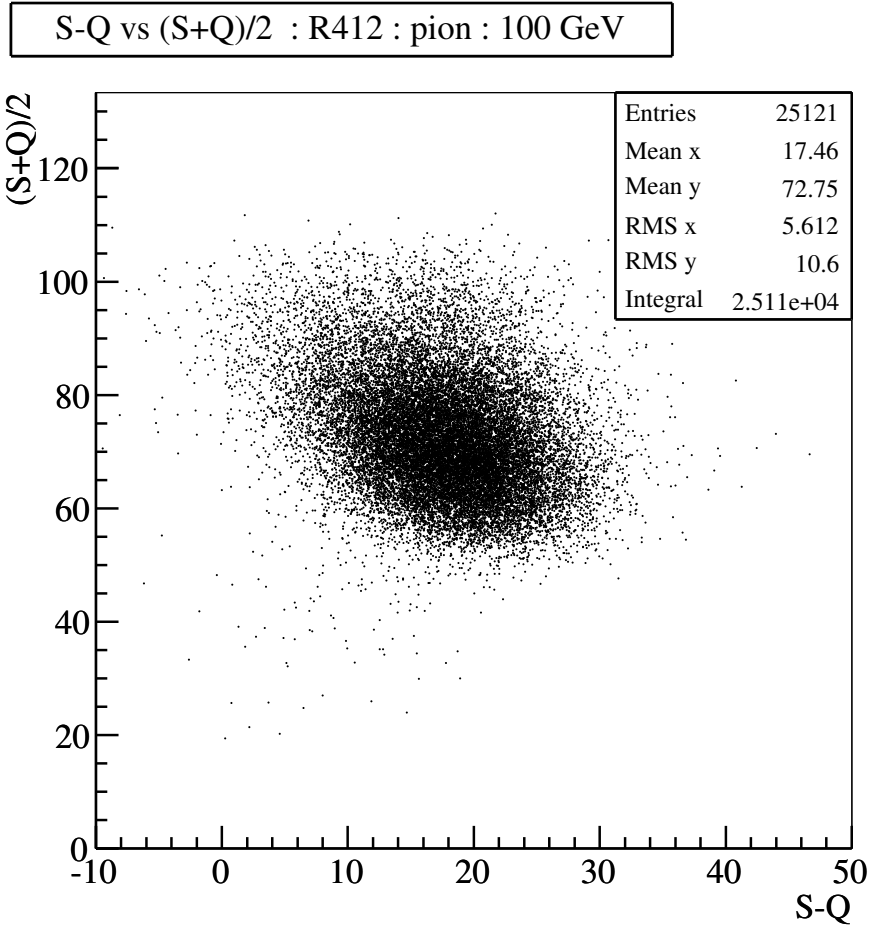


Figure 21: For 100 GeV pions, the distribution of $(S+\check{C})/2$ vs. $(S-\check{C})$ shows 5 events in the muon acceptance region, $0 < (S+\check{C})/2 < E_\mu/4$ and $-1 \text{ GeV} < (S-\check{C}) < 5 \text{ GeV}$, for a pion-to-fake-muon rate of $\sim 5/25K \sim 0.2 \cdot 10^{-3}$.

were used in this electron measurement, so we have yet to determine the ultimate electron energy resolution in this calorimeter.

The electron profiles are very narrow in these 7.2-cm wide channels, and electron identification is easily made with a width requirement. These measurements of energy resolution are described in [14], and the electromagnetic shower profiles are presented in [16], also available at the website[13].

Finally, the energy resolution for electrons can be marginally improved by averaging the (partially independent) Q and S measurements. We have not done this; however, there are statistical techniques that allow an optimum estimate from multiple measurements, but this is not a big gain. The proposed improvements (Sec. 4.3) will incorporate a fiber geometry that will intinsically improve the e energy resolution

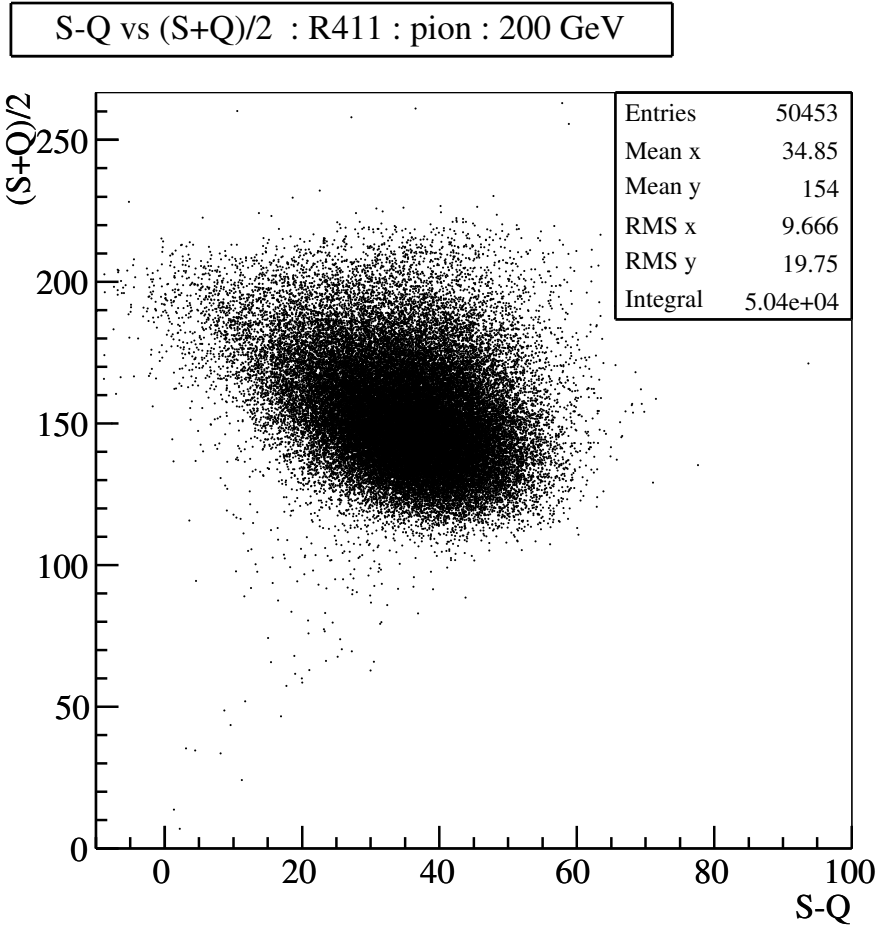


Figure 22: For 200 GeV pions, the distribution of $(S+\check{C})/2$ vs. $(S-\check{C})$ shows 4 events in the muon acceptance region, $0 < (S+\check{C})/2 < E_\mu/4$ and $-1 \text{ GeV} < (S-\check{C}) < 5 \text{ GeV}$, for a pion-to-fake-muon rate of $\sim 4/50K \sim 0.1 \cdot 10^{-3}$.

5.3 Photons (γ)

Photons are measured by the strict absence of a track in the tracking detectors and the presence of a narrow single-shower in the calorimeter. The main backgrounds are higher energy $\pi^0, \eta \rightarrow \gamma\gamma$ decays.

The TPC with its detailed tracking capability allows any electromagnetic shower in the calorimeter to be associated or not associated with charged tracks, and this $e - \gamma$ discrimination will be excellent, but limited by the position resolution of electromagnetic showers in the calorimeter. This limitation can be addressed with a finely segmented crystal, dual-readout EM calorimeter section in front of the fiber calorimeter, Sec. 4.3.

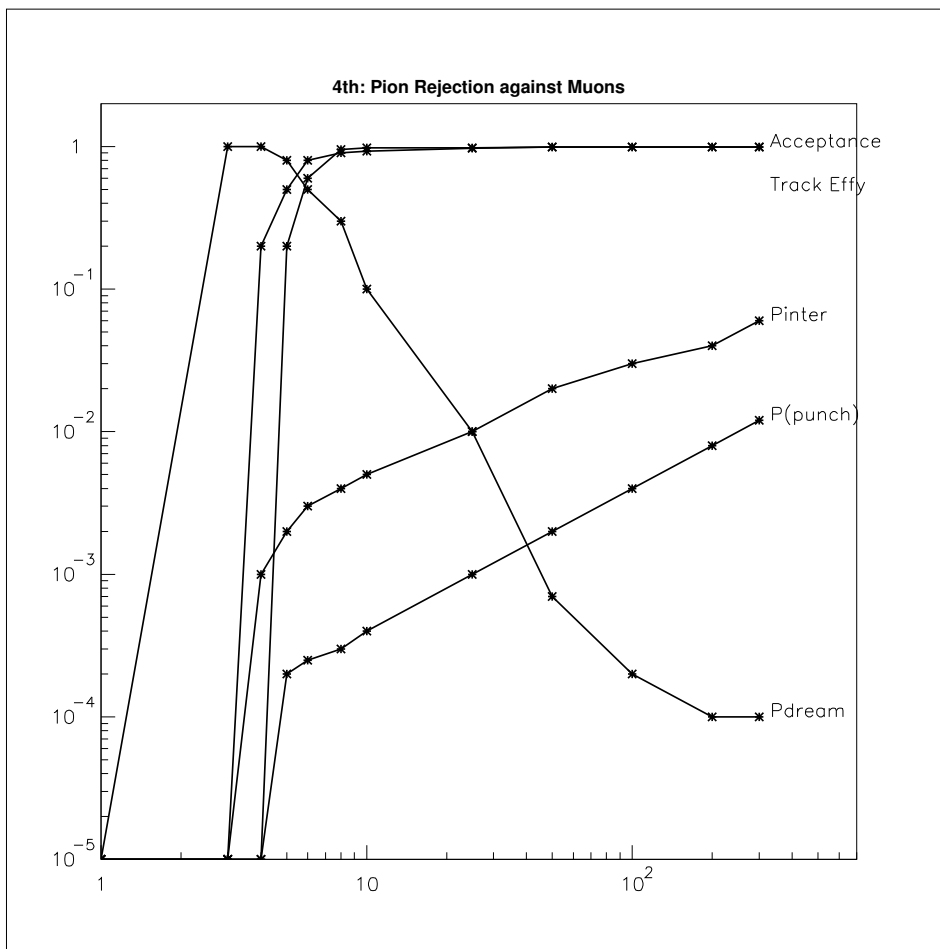


Figure 23: The numbers in Table 1 are plotted.

5.4 Muons (μ)

Muons are measured in the tracking detectors (momentum), identified and tagged in the calorimeter (difference of scintillation and Čerenkov), and again identified and momentum analysed in the muon system.

A detailed analysis of the muon data in DREAM is presented in [15]. The distributions of scintillation and Čerenkov signals for muons tagged in a 200 GeV π^- beam are shown in Fig. 10

A high energy muon will lose energy by dE/dx in addition to stochastic energy loss due to bremsstrahlung and pair production, the probability of which increases logarithmically with energy. In this dual readout calorimeter, the electromagnetic showers generated by bremsstrahlung and pair production are measured by both the scintillating fibers and the quartz fibers, whereas the dE/dx energy loss is measured only by the scintillating fibers. The quartz Čerenkov fibers capture zero light from a muon aligned with the fiber axes since the Čerenkov angle is larger than the numerical aperture capture angle of the fiber.

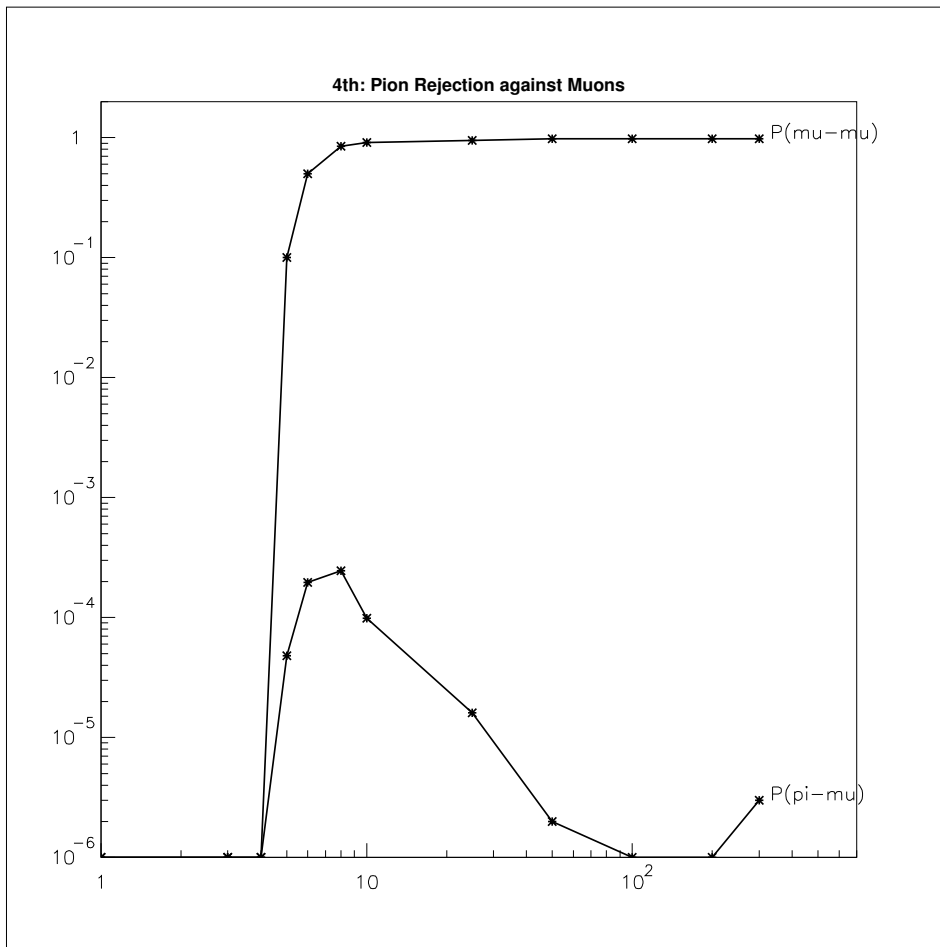


Figure 24: The numbers in Table 2 are plotted, the total probabilities for muon identification and pion mididentification as a muon are shown.

Thus, the difference of the S and Q signals measures just the dE/dx of the muon and is a constant, with resolution fluctuations, for each muon. We have found this to be the case, as shown in Fig. 11. As a side note, this is the first measurement that separates the ionization and radiation processes in muon energy loss.

A muon is momentum measured in the TPC, tagged by (S-C), its bremsstrahlung and pair production EM energy is measured to $\sigma_E = 20\%\sqrt{E}$ inside the calorimeter, and it is again momentum measured in the muon B-field region. We have not done hadron punch-through studies to assess the need for an additional non-magnetic absorber to further discriminate μ from π punch through.

Overall, a 100 GeV muon is measured to about 1% at each stage, including a 1% EM energy measurement for a 20 GeV EM energy deposit inside the calorimeter.

5.5 Missing transverse momentum (ν)

If every jet in an event is measured with high precision, the missing neutrino four-vector is known by subtraction to a precision about half as good as the individual jet and particle precisions. Therefore, we expect to be able to tag a missing ν momentum vector, excepting missing momenta in the forward region.

5.6 Jet "Mass" (optional section)

A precision near 2% on jets demands that we understand, and be able to use, all four components of the measurement of a jet in a calorimeter. The sum of the vectors of all calorimeter towers is the 3-momentum of the jet, \vec{P} . Summing the scalar energies is the energy, E , and $M = \sqrt{E^2 - \vec{P} \cdot \vec{P}}$ is a mass that basically measures the transverse spread of the calorimeter towers with respect to the jet direction. It is not clear how this jet mass will be useful in physics analyses, but we might expect it to become important for high precision mass reconstruction using jets.

6 Near-Term R&D

Secs. 6.1 and 6.2 are mainly the LCRD proposals [11, 10] on neutron measurement, photonconverter studies and study of a separate EM section in front of a DREAM-like calorimeter, and both are an integral part of this concept.

6.1 Measuring the neutrons: binding energy loss fluctuations

The success and the simplicity of the dual readout calorimeter has led us to ask the obvious question: What is the next largest fluctuation in a hadronic shower, after the electromagnetic fraction fluctuation, and how can we measure it? This is the subject of an LCRD proposal[11].

The next largest is the fluctuation in the binding energy losses in nuclear break-up, and this is proportional to the number of 1-2 MeV neutrons in the calorimeter medium. Neutrons in this energy range are most easily measured by presenting them with a hydrogenous medium, usually a hydrocarbon, and then measuring the proton elastic recoils from the $np \rightarrow np$ scatters. The kinematics of equal-mass elastic scattering are that the neutron loses one-half of its kinetic energy per collision, *i.e.*, the proton recoils are in the MeV range and easily detected in, for example, a plastic scintillator that is high in hydrogen content. This is the most obvious technique for measuring the neutrons. We list four methods we are considering:

1. Read out the time history of a fiber

MeV neutrons are slow, $v_n \sim \sqrt{2T/M_n} \sim 0.05c$, so $np \rightarrow np$ scatters will show up later in the scintillation fibers. This is illustrated in Fig. 13. We can use the Analog Transient Waveform Digitizer (ATWD)[22] to achieve time buckets of

1-2 ns lasting for 200 ns. We would also read out the Čerenkov fibers for three reasons: late e^\pm light that might be confused with $np \rightarrow np$ can be tagged by simultaneous light in the Čerenkov fibers; we have found in DREAM data that the e^\pm lineshape is time-dependent[17]; and, $nA \rightarrow A^* \rightarrow \text{multi-}\gamma\text{s}$ will be part of n signal. Finally, Čerenkov time-readout will also be a monitor of the entire interbunch activity and serve as a baseline.

2. A third non-hydrogenous fiber

Have both hydrogenous (S_H) and non-hydrogenous (S_Z) scintillating fibers. The hydrogenous fiber will see all charged particles plus the MeV protons from neutron recoil ($np \rightarrow np$). The non-hydrogenous fibers will see only the charged particles. The light yield will almost for sure be less in the non-hydrogenous fibers, so the number of neutrons will be proportional to

$$\text{number of neutrons} \propto S_H - a \cdot S_Z.$$

where the coefficient a may be substantially less than 1 due to low scintillating efficiency.

3. A third neutron-sensitive fiber

Have a third fiber that is explicitly sensitive to neutrons, such as Li-loaded or B-loaded glasses or liquids[11].

4. A third fiber with a very different Birks' constants

Have two hydrogenous scintillating fibers with very different Birks' constants and therefore different responses to low energy proton ionization[23]. The Birks' constant parameterizes the degree of suppressed ionization of heavily ionizing low energy particles (in this case, protons) due to recombination of the ionization electrons. A review of such constants reveals that it is possible, but difficult, to get scintillators with widely different Birks' constants.

The second and the fourth methods are weak since the neutron signal is proportional to a difference of two fluctuating measurements. The second method is more robust, but suffers from two problems: the scintillator may be liquid, and the time response is nuclear and may be slow relative to 100 ns. The first method may be costly, and will also lose some of the more prompt neutrons, as is evident in Fig. 13.

The performance of a "triple readout" calorimeter can be calculated, maybe with GEANT 4, but only reliably calculated if the nuclear physics of binding energies, energy levels, and neutron yields in MeV neutron capture and nuclear break-up are done correctly in GEANT 4. We can estimate the size of these fluctuations and then estimate the resolution enhancement if we include this third measurement in the hadronic energy estimate.

Finally, all neutron measurement schemes must be tested, with a view to possibly a combination of methods, *e.g.*, time-readout of hydrogenous and non-hydrogenous fibers. We have already learned from the 2004 beam test of the

DREAM module that there is important information contained in the time structure of a signal, and if we measure also the time history, then we have space, time, and EM/hadron information for reconstruction.

6.2 Photoconverters

We have begun a study of photoconverters for the readout of optical fibers[10]. We seek several improvements over the R580 PMT (1.5-inch, 10-stage) we used in the DREAM test beam: smaller and more compact; smaller effective photocathode area; insensitive to magnetic fields; and, lower cost. The GLD group is making substantial progress on Multi pixel Photon Counters (MPC)[6].

The MPC, earlier called a silicon PMT (SiPMT), consists of about 10^3 Si pixels per mm^2 operating in a limited Geiger mode at a gain of 10^6 . Each pixel is binary, but the high density of pixels ensures that the hit probability per pixel is much less than one, and so that the resulting response is very close to linear. Tests have shown [6] that gain, noise, time resolution, single-photon detection for calibration, operation in a magnetic field, and stability under temperature and voltage variations, and small bias ($\sim 50\text{V}$) make them superior to PMTs. Only the dynamic range limitation of about 10^3 is worse, but acceptable for this purpose.

6.3 Manufacture of two ILC-type modules

The next beam test will [7] likely be of two ILC-type calorimeter modules that are linked together and with the geometry we consider best for a full, 4π ILC detector. The main parameters of these modules are

- W, tungsten: for reasons of compactness, calorimeter depth, calorimeter performance, minimization of attenuation fluctuations, leakage suppression and mechanical strength;
- Flat plates with U-shaped grooves: construction will be easier if the W is in the form of mm plates with grooves to accept the three fibers. However, a metal mass with single holes for single fibers may be easier to load, but more difficult to construct. Stacked plates with grooves, resulting in stuffable holes, may be an easy option;
- Truncated hexagon modules: a geometry that allows a full 4π assembly from individual (and nearly identical) modules is that of a hexagonal pyramid with the top cut off;
- Photoconverters described in Sec. 6.2;
- Fiber types: clear plastic (Čerenkov fiber), non-hydrogenous glass scintillator (scintillation dE/dx fiber), and plastic scintillator (n fiber); and,
- Time history readout of the clear and scintillating fibers, described in Sec. 4.3.1.

The three-fiber test module will serve as a test of the triple readout idea, as a first prototype for the final modules, as a model for the mechanical issues, and as a test of the projective and non-projective fibers in a 4π detector.

One scheme for its construction is to start with 2-3 mm thick flat tungsten (W) plates with rolled or milled "U" shaped grooves of the same spacing as the plate thickness. All the grooves on each plate are loaded with three fibers, which are also grouped into ferrule bundles for the separate photoconverters. This complete, the next W plate is placed on top, and all the grooves loaded with fibers. This is fine work since the fibers will be likely 800- μm diameter and the grooves are closely spaced. Relaxing the thickness (and therefore the groove spacing) from 2 to 3 mm makes for easier assembly and quadratically fewer fibers, but worse resolution. The issue will be the spatial non-uniformity, constant terms in the energy resolution, the Moliere radius of W, and other basic physics performance issues. These are relatively easy problems for GEANT 4.

This plate-stacking procedure will allow us to load fibers up to the edges of modules for spatial uniformity across the boundaries between modules. It will also allow parallel assembly of modules. This group has substantial experience designing, assembling and testing 36 6-tonne modules for the Hadronic Forward (HF) calorimeters of the CMS facility at CERN.

Concern A concern to be tested is the known Zeeman enhancement of scintillation efficiency in a magnetic field.

7 Physics Event Analysis DRAFT SECTION

7.1 IVCRoos analysis system

Two 150 GeV electrons into the calorimeter, both EM crystal and fiber hadronic sections, of the 4th concept are shown in Fig. 25.

7.2 Event analysis

This unique calorimeter and comprehensive TPC for tracking allow us to perform detailed analyses of events. The separation of the two-quark (q) final states W and Z from the QCD background of gluons (g) will depend on the finely segmented and precise calorimetry and tracking.

Identification and reconstruction of jets The reconstruction of jet four-vectors depends on the definition of the jet, the sum over the energies in identified calorimeter towers, and the spatial locations of the centroid of the jet in the calorimeter system and the vertex origin of the particles of the jet. The separation of q from g jets is one important capability.

TRACK VARIABLES: W s and Z s are 40-45 GeV jets in the W, Z center-of-mass, and these objects differ from more energetic gluons in a number of ways. For WW

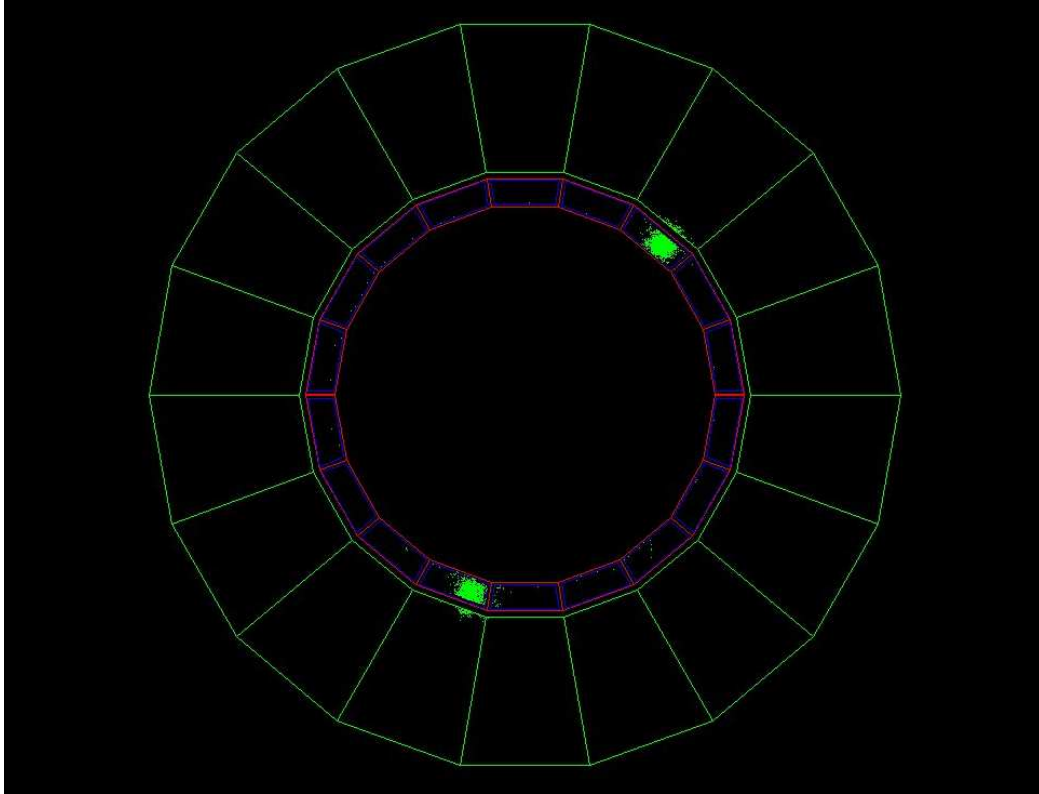


Figure 25:

final states, whatever q - g discrimination factor is achieved here will be raised to the fourth power in a WW physics problem.

1. Number of tracks:
2. Moments of track distributions: dN/dr and dE/dr where r is the jet shower axis;
3. Width and shape of the track and energy patterns:
4. Invariant jet "mass" and contributions to mass as a function of r ;

A crude estimate of the g -jet rejection relative to the q -jet efficiency from these methods is about 3-5. Therefore, in a process like $WW \rightarrow jjjj$ the QCD rejection is ~ 200 -300.

TWO-JET VARIABLES: The W and Z are quantum states with known masses and, for unpolarized ensembles, their two-body decays are isotropic in their centers-of-mass. In contrast, the radiation of a gluon from either a q or a g is a bremsstrahlung process quite unlike an isotropic decay of a massive state.

1. Decay cosine in the 2-jet cm:
2. Invariant mass of 2-jet system:

3. Distribution of mass within the 2-jets:
4. Energy and track densities and their distributions:

WHOLE EVENT VARIABLES: A WW event is generated by a EW process with few or no QCD internal or external lines. Therefore, the amount of hadronic debris in such an event should be smaller than in typical QCD gg collisions.

1. Number of tracks (or, mini-jets) between supposed W, Z jets:
2. Track distributions relative to the jets of the event:
3. Energy in calorimeter between jets:
4. Overall extra "mass" between jets.

Whole event variables depend critically on the collider environment with respect to multiple interactions, and the quality of the detector with respect to cracks and instrumental inefficiencies. We guess that an overall QCD rejection relative to $WW \rightarrow jjjj$ efficiency is about 10.

These relative rejection factors will be somewhat correlated, but we guess that an overall QCD 4-jet rejection relative to $WW \rightarrow jjjj$ can be as high as $\sim 8 \cdot 10^5$.

8 Personnel, Schedule, Time and Cost Estimates

We expect to answer most of these questions about the final configuration of an ILC experiment within the next few years, that is, the decision on the number of fibers; the decision on the time-history readout; the decision on the tracking detector (TPC); and, the design of the vertex and muon systems.

The calculations and a beam test of a time-history fiber calorimeter, or of a triple readout calorimeter, will be the most time consuming, but we have many years of experience with fiber calorimeters, and we anticipate few problems. Indeed, the calculations of time-history readout are already underway and look promising.

The decisions about the TPC will profit from the varied efforts worldwide [19] on the design and construction of several TPCs at different machines, but especially the TPC of the Large Detector Concept (LDC) group[20].

Budget This detector concept embodies the ideas and results of the successful DREAM tests and therefore represents a substantial return on the quite small investment given to the DREAM group by the Advanced Detector Research (ADR) program of DoE. It properly represents a success of the ADR program of the Department of Energy.

We will estimate a cost for the calorimeter by scaling from the costs of the DREAM module. The TPC, Si pixels and strips, and the Muon system have not been costed by us yet, but will be in line with those estimates of other groups.

Supporting Proposals We will pursue the following proposals.

- One postdoc per institution (approximately \$100K/y for ISU, TTU, *etc.*;
- KOSEF proposal to Korean Science Foundation; and,
- Support from ISU, TTU and other participating institutions.
- NSF proposal \$100K/y to support high school students and teachers working on this detector, hopefully with Tom Jordan in charge;

We have a long history of bringing young people into our groups, starting with QuartNet and continuing into the direct involvement of undergraduate physics majors and high school students working on both instrumentation and physics problems in our labs. This ILC detector development will be a perfect setting for high school students and physics majors from our universities to spend entire summers working on building, bench testing, beam testing, writing software, and calculating.

Personnel The contacts are listed below, along with others now working on the 4th Concept:

Contact	John Hauptman	hauptman@iastate.edu	515-451-0034
R&D Contact	Nural Akchurin	Nural.Akchurin@ttu.edu	806-470-6698
Costing Contact	Nural Akchurin		
MDI Contact	John Hauptman		
Calorimeter R&D	Richard Wigmans	wigmans@ttu.edu	806-742-3779

Others working on this concept and their areas of interest and work::

Sorina Popescu Laura Radulescu	Sorina.Popescu@cern.ch	TPCs engineering
Aldo Penzo	penzo@cern.ch	calorimeter
Giovanni Pauletta		muon, all
Muzaffer Atac Robert Wands G.P. Yeh	matac@fnal.gov wands@fnal.gov gpyeh@fnal.gov	chambers muon magnetic field physics
Heejong Kim Sungwon Lee Richard Wigmans Mario Spezziga	Heejong.Kim@ttu.edu wigmans@ttu.edu Mario.Spezziga@cern.ch	calorimeter calorimetry calorimeter
Oleksiy Atramentov Sehwook Lee Jerry Lamsa Robert Schoene Matt Stemper German Valencia	oleskiy@fnal.gov swlee34@iastate.edu Jerry.Lamsa@cern.ch schoene@iastate.edu stemperm@iastate.edu valencia@iastate.edu	calorimeter calorimeter simulation magnetic field top mass physics coordinator
Sunghwan Ahn Tae Jeong Kim Kyungsei Lee Sung Keun Park	shahn@kodel.korea.ac.kr tjkim@fnal.gov kslee0421@korea.ac.kr sungpark@korea.ac.kr	calorimeter calorimeter muon TPCs, muon
Emanuela Cavallo Vito Di Benedetto Corrado Gatto Franco Grancagnolo Anna Mazzacane Roberto Perrino	Emanuela.Cavallo@inf.nle.it vito.dibenedetto@inf.nle.it corrado.gatto@inf.nle.it franco.grancagnolo@inf.nle.it roberto.perrino@inf.nle.it	muon calorimeter software system tracking pattern recog.
Michael Gold John Matthews John Strologas		pixel, TPC
Sezen Sekmen Efe Yazgan Mehmet Zeyrek		

Simulations GEANT 4 is clearly the biggest hole in this description. We are working on a simple implementation at ISU. Of course, extensive work on fiber calorimeters, dual-readout calorimeters and TPCs has been performed at ISU over the years, but this was all with GEANT 3. We realize the importance of this and are appropriately concerned about the timeliness of the work.

References

- [1] "Dual-Readout Calorimetry for High-Quality Energy Measurements", October 2001, proposal to Advanced Detector Research program of DoE, R. Wigmans, *et al.*. The website containing the proposal, all papers and figures is <http://www.phys.ttu.edu/dream>, which can be linked from <http://highenergy.phys.ttu.edu>. The main ideas were first discussed in detail by Wigmans, "Quartz Fibers and the Prospects for Hadron Calorimetry at the 1% Resolution Level", Proceeding for the 7th International Conference on Calorimetry in High Energy Physics, Tucson, 1997.
- [2] The first mention of this dual-readout as a means to improve hadronic energy resolution was made by Paul Mockett, "A Review of the Physics and Technology of High-Energy Calorimeter Devices", proceedings of the *11th SLAC Summer Institute on Particle Physics*, July 1983, SLAC Report No. 267. David Winn proposed readout of scintillation and ionization in LAr, *IEEE Trans. Nucl. Sci.* **NS-36**, 334. A detailed discussion and calculation of a dual readout calorimeter was made by Erik Ramberg, "Recent Developments in High-Speed, Non-Sampling Electromagnetic Calorimetry", March 1990, Fermilab-Conf-90/46.
- [3] To name a few: (*i*) the absolute energy calibration with 40 GeV e^- was implemented by adjusting the high voltages to the 38 PMTs, on the fly by eyeball interpolation, to put the mean of the energy distribution at a fixed ADC count; (*ii*) the center channel and the first ring of six channels had pure quartz for the Čerenkov fibers while the outer ring of 12 channels had plastic fibers with a numerical aperture 1.5 times larger, and this spatial non-uniformity can contribute a small fluctuation to the overall energy driven by lateral fluctuations in hadronic shower development; (*iii*) the finite width of the module, only 30 cm, introduces a small variation in leakage with energy; (*iv*) although care was taken in the construction of the module, the cleaving of fibers and light collection uniformity at the 0.5% level was not attended to; and, (*v*) although the calibration with 40 GeV e^- was checked again during the one-week run, no deliberate attempt was made to monitor or control time-dependent variations. This is all in keeping to the stated aim of testing the dual readout idea, not in attaining the best possible energy resolution.
- [4] "Scintillating Fiber Calorimetry", M. Livan, V. Vercesi, and R. Wigmans, CERN 95-02, 28 February 1995; also, R. Wigmans, *NIM A* **259** (1987) 389; and, E. Bernardi, *et al.*, *NIM A* **262** (1987) 229.
- [5] R. L. Gluckstern, "Uncertainties in Track Momentum and Direction, Due to Multiple Scattering and Measurement Errors" *Nucl. Instrum. and Methods* **24** (1963) 381.
- [6] Multi pixel Photon Counter (MPC), manufactured by Hamamatsu; originally developed at the Moscow Engineering and Physics Institute, reported by Dol-

goshin, *et al.*, at Beaune, 2003, as the silicon PMT, or SiPMT. Talk by T. Takeshita, for the Global Large Detector (GLD), report at the Snowmass Meeting, 2005, as part of the R&D for the GLD Muon system. These devices are spectacular, with a potential weakness that the high gain of $\approx 10^7$ is a strong function of both bias voltage and temperature.

Also, talk by H. Matsunaga on GLC calorimeter photosensors and electronics, "Electronics for GLD Calorimeter", Snowmass 2005.

- [7] Erik Ramberg, *Linear Collider Workshop*, Paris, April 2004; discussion of Fermilab beams to the Meson Lab up to 120 GeV, pions up to 100 GeV.
- [8] Jim Strait, private communication. Fermilab hosts a large and productive silicon detector laboratory.
- [9] The scintillating fibers are SCSF-81J, produced by Kuraray Co. Ltd., Tokyo, Japan; the clear plastic (Čerenkov) fibers are Raytela PJR-FB750, produced by Toray, Japan.
- [10] "Dual-Readout Calorimetry for the Linear Collider", Akchurin, Carroll, Kim, Wigmans, Paar, Penzo, Hauptman, Lamsa, LCRD proposal submitted Feb. 2005.
- [11] "Ultimate Hadron Calorimetry", Akchurin, Carroll, Kim, Wigmans, Paar, Penzo, Hauptman, Lamsa, LCRD proposal, Feb. 2005.
- [12] "Hadron and Jet Detection with a Dual-Readout Calorimeter", N. Akchurin, *et al.*, *Nucl. Instrum. and Methods* **A537** (2005) 537-561.
- [13] All DREAM papers and all figures are accessible at <http://www.phys.ttu.edu/dream>, and also <http://highenergy.phys.ttu.edu>.
- [14] "Electron Detection with a Dual-Readout Calorimeter", N. Akchurin, *et al.*, *Nucl. Instrum. and Methods* **A536** (2005) 29-51.
- [15] "Muon Detection with a Dual-Readout Calorimeter", N. Akchurin, *et al.*, *Nucl. Instrum. and Methods* **A533** (2004) 305-321.
- [16] "Comparison of Scintillation and Čerenkov Light in High-energy Electromagnetic Profiles", N. Akchurin, *et al.*, *Nucl. Instrum. and Methods* **A548** (2005) 336-354.
- [17] "Separation of Scintillation and Čerenkov Light in an Optical Calorimeter", Accepted, *Nucl. Instrum. and Methods* **A**, in press.
- [18] "Quartz fibers as active elements in detectors for particle physics", N. Akchurin and R. Wigmans, *Rev. Sci. Instr.* **74** (2003) 2955.
- [19] *Time Projection Chamber Symposium*, Lawrence Berkeley National Laboratory, 17 October 2003; and, the many efforts in designing and testing TPCs in the GLD and LDC communities of the ILC.

- [20] The Large Detector Concept (LDC) and the Global Large Detector (GLD) are both designing large volume TPCs.
- [21] A. Savoy-Navarro, LPNHE, Universite Pierre & Marie Curie.
- [22] The Analag Transient Waveform Digitizer (ATWD) has been developed at LNBL for NESTOR and other applications. This ASIC can be further developed for this application, firstly, by the addition of 512 switching capacitors so that a total time of $1 \mu s$ can be digitized at 0.5 GHz for the calorimeter fiber bundles, or $50 \mu s$ can be read out at 10 MHz for the TPC. Some references: "A Multi-GHz Multi-Channel Transient Waveform Digitization Integrated Circuit", Stuart Kleinfelder, *IEEE Procs.*, Nov. 2002 (also, thesis, May 2002, UC Berkeley).
- [23] Kurtis Johnson, Florida State University, private communication. .